

**Assessing the Range of Enzymatic and Oxidative Tunability
for Biosensor Design**

Journal:	<i>Journal of Materials Chemistry B</i>
Manuscript ID	TB-REV-11-2019-002666.R1
Article Type:	Review Article
Date Submitted by the Author:	01-Feb-2020
Complete List of Authors:	Schunk, Hattie; University of Texas at Austin Cockrell School of Engineering, McKetta Department of Chemical Engineering Hernandez, Derek; University of Texas at Austin Cockrell School of Engineering, Department of Biomedical Engineering Austin, Mariah; University of Texas at Austin Cockrell School of Engineering, McKetta Department of Chemical Engineering Dhada, Kabir; University of Texas at Austin Cockrell School of Engineering, Department of Biomedical Engineering Suggs, Laura; University of Texas at Austin Cockrell School of Engineering, Biomedical Engineering Rosales, Adrienne; University of Texas at Austin Cockrell School of Engineering, McKetta Department of Chemical Engineering

ARTICLE

Assessing the Range of Enzymatic and Oxidative Tunability for Biosensor Design

Received 00th January 20xx,
Accepted 00th January 20xx

Hattie C. Schunk^{a,b}, Derek S. Hernandez^a, Mariah J. Austin^b, Kabir S. Dhada^a, Adrienne M. Rosales^{b*} and Laura J. Suggs^{a*}

DOI: 10.1039/x0xx00000x

Development of multi-functional materials and biosensors that can achieve an *in situ* response designed by the user is a current need in the biomaterials field, especially in complex biological environments, such as inflammation, where multiple enzymatic and oxidative signals are present. In the past decade, there has been extensive research and development of materials chemistries for detecting and monitoring enzymatic activity, as well as for releasing therapeutic and diagnostic agents in regions undergoing oxidative stress. However, there has been limited development of materials in the context of enzymatic and oxidative triggers together, despite their closely tied and overlapping mechanisms. With research focusing on enzymatically and oxidatively triggered materials separately, these systems may be inadequate in monitoring the complexity of inflammatory environments, thus limiting *in vivo* translatability and diagnostic accuracy. The intention of this review is to highlight a variety of enzymatically and oxidatively triggered materials chemistries to draw attention to the range of synthetic tunability available for the construction of novel biosensors with a spectrum of programmed responses. We focus our discussion on several types of macromolecular sensors, generally classified by the causative material response driving ultimate signal detection. This includes sensing based on degradative processes, conformational changes, supramolecular assembly/disassembly, and nanomaterial interactions, among others. We see each of these classes providing valuable tools toward coalescing current gaps in the biosensing field regarding specificity, selectivity, sensitivity, and flexibility in application. Additionally, by considering the materials chemistry of enzymatically and oxidatively triggered biomaterials in tandem, we hope to encourage synthesis of new biosensors that capitalize on their synergistic roles and overlapping mechanisms in inflammatory environments for applications in disease diagnosis and monitoring.

1 Introduction and Motivation

1.1 The Grand Challenge in Biosensing: Achieving a Specific *In Situ* Material Response

Physiological and pathological processes are inherently dynamic and are tightly linked to the fluctuation of a variety of biological conditions (*e.g.* pH, temperature, redox state, chemical species, etc.). Stimuli-responsive biomaterials have long been investigated to elicit a specific response to these biological signals in order to deliver therapeutic or diagnostic agents in a spatially and temporally controlled manner.^{1–3} In particular, enzymatic⁴ and oxidative⁵ mechanisms are ubiquitous throughout life; hence, we have a range of materials at our disposal that respond to these stimuli.^{6–26} However, a key challenge has been to engineer materials that selectively and accurately respond to one type of mechanism (*e.g.* a specific oxidant or enzyme) or respond to both mechanisms synergistically, while also maintaining stability *in vivo*. This is not

necessarily due to a lack of understanding of individual enzymes and oxidants in physiological and pathophysiological contexts, but a tendency to overlook the contribution of *both* enzymatic and oxidative susceptibility when it comes to biomaterial design.

Many reviews on biologically triggered materials have focused exclusively on enzymatic^{4,6,20,22,25,27} and oxidative^{9–11,13,14,26,28} response mechanisms, significantly overlooking contributions from off-target species. Now, more than ever, there is increased knowledge of the chemistry of physiologically relevant reactive oxidants^{11,29–33} and enzymes,^{34–36} how they interact with other biological molecules,^{37,38} how they contribute to signalling pathways,^{32,36,39–41} and evidence linking these events to distinct pathological conditions.^{20,21,38} Given this knowledge, the next generation of biosensors will ideally achieve detection with high specificity, selectivity and sensitivity to their target, largely undisturbed by other processes in the biological environment.⁴⁴ For clarity, we adopt a distinction between the terms ‘selectivity’ and ‘specificity’ established by Haedke *et al.*⁴⁵ Namely, selectivity describes the ability for a probe to “choose” one single species among many (*e.g.* oxidant vs. enzyme), whereas specificity is a measure of the rate of false positives. This means highly specific probes have little off-target effects, but may be modified by multiple different sub-species if they have common chemical functionality. Designing a system that uniquely interacts with and responds to

^a Department of Biomedical Engineering, University of Texas at Austin, Austin, TX 78712, USA. E-mail: suggs@utexas.edu

^b McKetta Department of Chemical Engineering, University of Texas at Austin, Austin, TX 78712, USA. E-mail: arosales@che.utexas.edu

[†] Footnotes relating to the title and/or authors should appear here.

Electronic Supplementary Information (ESI) available: [details of any supplementary information available should be included here]. See DOI: 10.1039/x0xx00000x

specific enzymes and oxidants to produce an accurate, informative and detectable signal in this way requires a multidisciplinary

approach guided by consideration of the interplay between materials chemistry and biological effects. In this review article, we aim to provide a portfolio of approaches for designing biomaterials triggered by tightly linked enzymatic and oxidative inflammatory biomarkers. By connecting materials chemistry with inflammatory environments, we hope to inspire a comprehensive approach towards future biosensor design.

1.2 Inflammatory Environments: A Case for Oxidative and Enzymatic Sensing

Chronic oxidative stress^{11,29,31–33} and the dysregulation of proteases^{35,36} are considered important contributing factors to the etiology of inflammatory diseases such as cancer, neurodegeneration and cardiovascular dysfunction.^{29,31,36,46} As a result, reactive oxygen species (ROS), proteases (matrix metalloproteases, caspases, cathepsins etc.), catalytic enzyme pairs (phosphatases/kinases), as well as other oxidative and enzymatic species, serve as important inflammatory biomarkers of diseased cells, as well as triggers to facilitate desired changes in materials aimed to target these diseases.^{7,28} For detecting and sensing of these species in complex inflammatory environments, biosensors aim to take advantage of local abnormalities: for example, the upregulation of ROS associated with immune activation,^{29,30,33} or increased activity of cathepsins and other proteases in mediating extracellular matrix degradation in tumor metastasis.³⁶ However, the interplay and dysregulation between enzymatic and oxidative species are also important to consider. For example, ROS-induced activation of matrix metalloproteases (MMPs) promotes cancer cell migration,^{42,43} and oxidation at the catalytic site of protein tyrosine phosphatase (PTP) regulates intracellular inflammatory response cascades. Despite the contribution of these mechanisms to inflammatory disease pathology,^{37,38} a lack of accurate methods to differentially monitor the entire spectra of components encountered *in vivo* exists (**Figure 1A**). Developing systems capable of differentiating ROS and enzymes (ROS Selective Probes and Enzyme Specific Sensors, **Figure 1B**), as well as multi-responsive materials that respond to enzymatic and oxidative triggers in synergy (Multi-Responsive Materials, **Figure 1B**) would not only facilitate our understanding of their roles in disease pathology, but also contribute to the development of improved diagnostic and therapeutic strategies that more accurately define these diseases.

In light of these goals, this review aims to inspire the use of materials chemistry to design novel sensors that address a spectra of enzymatic/oxidative susceptibility *in tandem*. To accomplish this task, we first highlight current state-of-the-art oxidatively and enzymatically triggered biomaterials to draw attention to the range of synthetic tunability available in biomaterials fabrication. In doing so, we intend to establish a toolbox of macromolecular materials chemistries capable of interacting with the complex biological signalling underlying inflammatory disease with programmed

degrees of responsive behavior. Our hope is that these contributions will motivate the development of new, multi-functional materials, while keeping in mind current limitations and bringing to light mitigation strategies for optimal translation of materials with widespread applications in the detection, monitoring and treatment of inflammatory disease.

1.3 Oxidatively and Enzymatically Triggered Biomaterials: Key Components to Biosensor Design

In general, the design of a biosensor has three requirements: (1) it must have a responsive component, defined as the part of the sensor that recognizes the stimulus (*i.e.*, the enzymatic or oxidative trigger), (2) it must translate the action of the target to the rest of the material and (3) the translation has to cause a change in the overall properties of the material sensitive enough to elicit a detectable signal. Integration of these components into enzymatically and oxidatively triggered materials can be accomplished in a variety of ways, and is often concomitant with a higher order response.^{47–51} This can include the separation of materials caused by degradative processes, dynamic supramolecular assembly and disassembly of peptide chains, analyte-mediated interactions between nanoparticles, or swelling-induced conformational changes of materials. Although this is primarily mediated by only a few types of reactions (bond formation/cleavage, transfer/removal/addition of functional groups, and redox reactions), the material changes can be rather diverse, resulting in a number of material responses with detectable outputs that can be exploited in sensing applications.

Keeping this diversity of responses in mind, we have organized our discussion into four general categories based on the material response driving the sensing output. These responses include: (1) Degradative Processes, (2) Supramolecular Assembly/Disassembly, (3) Nanomaterial Interactions, and (4) Conformational Changes. We see each of these classes providing unique advantages and trade-offs when it comes to designing the “ideal” biosensor (**Figure 2**). For example, sensors based on material degradation, characterized by an irreversible separation of the biosensor components, are marked by high levels of sensitivity. Alternatively, sensors based on supramolecular self-assembly/disassembly, such as self-aggregating amphiphilic peptides, are characterized by inherent flexibility and the ability to sense dynamic behavior. Sensors based on analyte-mediated interactions of nanomaterials demonstrate high degrees of specificity due to their “by-design” target affinity, an attractive feature for multiplexed applications. Similarly, sensors based on conformational changes, such as swelling triggered by analyte-mediated hydrophobic to ϕ -philic exchanges, exhibit environment-dependent adaptability resulting from highly tunable chemistries. Although these classes are generalizations and inevitably find some overlap, we believe such organization will provide valuable insight for application in inflammatory disease sensing where the overlapping oxidative and enzymatic mechanisms necessitate an

extensive toolbox of material responses that intelligently interact with the complexity of the inflammatory environment in a variety of ways.

To give a snapshot of the extensive research in the area, we first provide a compilation of reports on oxidatively and enzymatically triggered biomaterial platforms (Tables 1 and 2) for detection of oxidative and enzymatic inflammatory biomarkers, specifically drawing attention to the responsive component, specific analyte, method of detection and level of sensitivity achieved. In regard to scope, we have focused primarily on biosensors relying on spectroscopic (SPR shift) or optical (fluorescence, luminescence) readouts— thus amenable to *in vivo* application due to their compatibility with photoacoustic (PA) and fluorescence imaging modalities. We have centered discussion on macromolecular sensors, excluding small molecular dyes and activity-based probes. Beyond sensors, we have chosen to highlight select examples using similar, important materials chemistry approaches for applications in drug delivery. By discussing what can be learned from these systems from a materials chemistry standpoint, we intend to demonstrate the numerous and versatile ways to achieve oxidative and enzymatic molecular recognition in the inflammatory environment, thereby providing valuable handles for future development of “by design” systems that can both detect and treat inflammatory disease.

ARTICLE

Table 1: Oxidatively Triggered Biomaterials

Responsive Component	Trigger**	Macromolecular Signal/Method of Detection++	Sensitivity (Lowest Reported Detection)
Detection Based on Degradative Processes			
Phenylboronic Esters/Ethers/Acids	H ₂ O ₂	Fluorescence, Nanoparticle size	2.5 μM ⁵² ; 50 μM ⁵³ ; 0.025 mM ⁵⁴ ; 5 μM ⁵⁵ ; 100 μM ⁵⁶ ; 0.1 mM ^{57#} ; 1mM ⁵⁸
Selenide groups	H ₂ O ₂ , O ₂ ^{•-}	Fluorescence, Nanoparticle size, Chromatography	50 μM ⁵⁹ ; 10 mM ^{9*} ; 0.1 v/v% ^{60,61} ; 1 mM ⁶² ; 0.1 mM ⁶³
Telluride groups	H ₂ O ₂ , O ₂ ^{•-}	Fluorescence, Nanoparticle size	0.1 mM ⁶³
Silicon	SIN-1 (ONOO ⁻ and [•] OH)	Fluorescence	1-2 mM ⁶⁴
Proline, Oxazoline, N-ethylglycine Oligomers	H ₂ O ₂ (+CuSO ₄)	Chromatography	[5 mM H ₂ O ₂ + 50 μM CuSO ₄ ; 1 mM SIN-1] ^{65,66} ; [0.5 mM H ₂ O ₂ + 50 μM CuSO ₄] ⁶⁷
Poly-D-Lysine	SIN-1 (ONOO ⁻ and [•] OH)	SPR, Fluorescence	5 μM ONOO ^{-68#} ; N/A ⁶⁹
Thiols/thiophenes	OH [•] (Fenton Reaction), ClO ⁻	Fluorescence, SPR	250 μM H ₂ O ₂ (in presence of Fe ²⁺) ⁷⁰ ; 0.7 μM ClO ^{-71#}
Polypropylene sulfide (PPS) / Thioethers/esters	H ₂ O ₂ , SIN-1 (ONOO ⁻ and [•] OH)	Fluorescence, Nanoparticle size	[0.0033 v/v% H ₂ O ₂ ; 100 μM SIN-1] ⁷²
Silver (Ag)	H ₂ O ₂ , HOCl	SPR	30-100 μM ⁷³ H ₂ O ₂ ; 0.2 mM HOCl ⁷⁴ ; 100 μM ⁷⁵
Polythioketal	O ₂ ^{•-} ; H ₂ O ₂ , KO ₂	Fluorescence, Chromatography, Nanoparticle size, Luminescence	100 mM H ₂ O ₂ ⁷⁶ ; [10mM KO ₂ /H ₂ O ₂] ⁷⁷ ; [400 mM+3.2 CuCl ₂] ⁷⁸ ; 100 μM H ₂ O ₂ ⁷⁹ ; N/A ⁸⁰ ; 10 mM H ₂ O ₂ ⁸¹ ; 400 mM H ₂ O ₂ and 3.2 μM CuCl ₂ ⁸² ; 100 μM KO ₂ ⁸³
Hyaluronic Acid;	OH [•] , ClO ⁻ , ONOO ⁻ , O ₂ ^{•-}	Luminescence, Fluorescence	[0.03 μM OH [•] ; 0.02 μM ClO ⁻ ; 0.06 μM ONOO ⁻ ; 0.1 μM O ₂ ^{•-}] ⁸⁴

Detection Based on Supramolecular Assembly			
Phenylboronic Acid	H ₂ O ₂	Fluorescence	1 mM ⁸⁵
Detection Based on Mediating Nanomaterial Interactions			
L-cysteine/thiols	H ₂ O ₂	SPR, Fluorescence	2 μM ⁸⁶ ; 1 μM ⁸⁷
Cerium ⁴⁺	H ₂ O ₂ , ONOO ⁻ , OCl ⁻ , •OH	Fluorescence	0.64 μM ⁸⁸
Detection Based on Conformational Changes			
Genetically Encoded Fluorescent Proteins (HyPer Probes/ E. coli protein OxyR)	H ₂ O ₂	Fluorescence, Bioluminescence	20 nM ⁸⁹ ; N/A ⁴⁰ ; 10 μM ⁹⁰ 20-30 nM ^{91,92}
Polypropylene Sulfide (PPS) / Thioethers/Esters	H ₂ O ₂ , ClO ⁻	Nanoparticle size, Fluorescence, SPR	[20 U/mL CPO or 5 U/mL MPO + 500 μM H ₂ O ₂ , and 2000 ppm NaOCl] ⁹³ ; 50 mM H ₂ O ₂ ⁹⁴
L-cysteine	H ₂ O ₂	Fluorescence, Nanoparticle size	0.1 v/v% ⁹⁵ ; 1 μM ⁹⁶ ; 10 nM ⁹⁷
Selenium, Tellurium, and Ferrocene-containing polymers	H ₂ O ₂	Fluorescence; Nanoparticle size	0.1 mM ⁹⁸ ; 100 μM ⁹⁹ ; N/A ¹⁰⁰ ; 450 mM ¹⁰¹ ; 100 μM ¹⁰²
Miscellaneous (i.e., energy transfer mechanisms/chemiluminescence)			
Phenylboronic Esters/Ethers/acids	H ₂ O ₂ , •OH, ONOO ⁻ , NO	Luminescence, PET, Fluorescence	0.5 μM H ₂ O ₂ ^{103#} ; 20 μM H ₂ O ₂ ^{104#} ; 0.75 μM H ₂ O ₂ ^{105#} ; 0.68 μM •OH ^{106#} ; 0.95 μM H ₂ O ₂ ^{107#} ; 100 μM ONOO ⁻¹⁰⁸ ; 100 μM H ₂ O ₂ ^{109#} ; 5 nM H ₂ O ₂ ¹¹⁰ ; 100 nM H ₂ O ₂ ¹¹¹ ; <1 μM H ₂ O ₂ ¹¹² ; 0.0335 μM H ₂ O ₂ ^{113#} ; 0.015 μM H ₂ O ₂ ¹¹⁴
Peroxalate esters	H ₂ O ₂	Luminescence, Fluorescence, Nanoparticle size	1 nM ¹¹⁵ ; 400 μM ^{116#} ; 500 nM ¹¹⁷
Silver (Ag), Gold (Au) and Copper (Cu) Nanocrystals	H ₂ O ₂ , ONOO ⁻ , OCl ⁻ , •OH	Luminescence, Fluorescence	0.3 μM H ₂ O ₂ ¹¹⁸ ; 30 nM ¹¹⁹ ; 0.1 – 0.5 μM H ₂ O ₂ ¹²⁰
Silicon	•OH (Fenton Reaction)	Luminescence, Fluorescence	0.97 μM ^{121#}

#indicates ratiometric, *indicates reversible

** **Triggers included:** Single Species: H₂O₂ (hydrogen peroxide), O₂⁻ (superoxide anion), KO₂ (decomposed to O₂⁻), •OH (hydroxyl radical), HOCl (hypochlorous acid); OCl⁻ (hypochlorite), and ONOO⁻ (peroxynitrite); Reactions: SIN-1 (decomposes to ONOO⁻ and •OH), Copper catalyzed reactions (H₂O₂ + CuSO₄ → •OH; H₂O₂ + CuCl₂ → •OH); Fenton Reaction (Fe²⁺ + H₂O₂ → Fe³⁺ + •OH + OH⁻)

++ **Methods of Detection:** Fluorescence (e.g., fluorescence spectroscopy, imaging, FRET); Surface Plasmon Resonance (SPR) (e.g., absorption spectroscopy, photoacoustic imaging); photoinduced electron transfer (PET); Luminescence (Chemi- or Bioluminescence); Nanoparticle size (analytical methods include Dynamic Light Scattering (DLS), electron microscopy, turbidity); Chromatography (e.g., High Performance Liquid Chromatography (HPLC), Liquid Chromatography- Mass Spectrometry (LC-MS), Gel permeation chromatography (GPC))

ARTICLE

2 Applications and Discussion: Oxidatively Triggered Materials

2.1 Targeting Inflammatory ROS/RNS

ROS play important physiological roles that contribute to a variety of diverse biological processes, for example: maintaining redox balance in cells, acting as secondary messengers, and contributing to cell growth and apoptosis.¹²² However, local oxidative stress (high levels of ROS) in cells leads to cellular dysfunction, ultimately contributing to abnormalities associated with inflammatory disease pathogenesis.^{11,29–33} As a result of the prevalence of ROS in inflammatory environments, exploiting these cell-generated species to trigger a response in biomaterial platforms has seen significant progress in recent years.^{8–15,26,28} However, to achieve accurate measurement and detection of these species for successful diagnosis of inflammatory disease, it is important to appreciate that ROS are not single entities, rather, a broad range of chemically distinct reactive species that individually and synchronously contribute to disease progression. ROS consist of H₂O₂ (hydrogen peroxide), O₂^{•-} (superoxide), [•]OH (hydroxyl radical), and OCl⁻ (hypochlorite ion). Reactive nitrogen species (RNS) such as NO (nitric oxide) and ONOO⁻ (peroxynitrite) are also important inflammatory biomarkers, among others.^{5,10–12}

Pioneering research in the field of ROS detection centered around the use of small molecular dyes (*e.g.*, dihydrodichlorofluorescein, and dihydrorhodamine).²⁶ Although these dyes set the groundwork for commercially available probes for detection of ROS *in vivo*, they are often insufficient in meeting the criteria of an “ideal” biosensor. The challenge in small molecule ROS sensing is that these systems employ non-specific mechanisms of activation, thus responding to multiple reactive species, as well as a complex milieu of other biological stimuli.^{30,122–124} Additionally, given the highly reactive and extremely short-lived nature of ROS/RNS, robust, sensitive detection on appropriate timescales is often difficult.¹²⁵ In recent years, considerable efforts on integrating ROS-sensitive small molecules into biomaterial platforms to improve their sensitivity, selectivity and specificity in application have led to major advancements in ROS sensing.¹²⁶ Despite progress, this field is still in its infancy.¹⁰ In Table 1, we list specific examples of ROS biosensors along with other examples of oxidatively triggered biomaterials in drug delivery in order to illustrate the breadth of materials chemistries available for future design of oxidatively triggered systems. Recalling Figure 2, these systems primarily fall into the following material response categories: degradative processes, supramolecular assembly/disassembly, nanomaterial interactions, and conformational changes. On the microscale, these changes are

mediated through oxidation of a chemical group (the responsive component), and detection can be achieved by a variety of signals (fluorescence, luminescence, chromatography, changing nanoparticle size, etc.) dictated by the final material response. In addition to those responses illustrated in Figure 2, Table 1 also includes a section on energy transfer and chemiluminescent based systems, as the high chemo-selectivity of these ROS-related reactions, which directly produce light from oxidation,¹¹² are commonly leveraged in ROS biosensors specifically. In this section, we will summarize select examples of functional results in both *in vitro* and *in vivo* sensing systems, as well as discuss their limitations from a materials chemistry standpoint. By taking this comprehensive approach, we aim to demonstrate the versatility of ways to achieve oxidative molecular recognition in order to make full use of the bio-orthogonality of these materials chemistries for sensing in inflammatory contexts.

2.2 Oxidatively Triggered Materials: Detection Based on Degradative Processes

Dating back many decades, research has revealed that various ROS-sensitive functional groups (*e.g.*, phenyl boronic acid/esters, diselenides, proline oligomers, polythioketals, etc.) undergo oxidation-induced degradation eventually leading to polymer backbone cleavage.^{10,13,15,16,28} Additionally, ROS-mediated oxidation resulting in the natural degradation of peptides and proteins has long been studied.^{127–131} Sensors intended to report ROS activity in living systems often take advantage of these oxidatively labile peptide linkers and chemical groups to cause the degradation of a material in a way that provides a detectable signal. Many of these systems utilize fluorescence-based methods of detection. For example, sensors based on fluorescence resonance energy transfer (FRET) have become a popular strategy for ROS detection in which separation caused by degradative processes leads to fluorescence recovery.^{55,59,78,80} Additionally, there are a number of systems in which fluorescent imaging agents are conjugated to ROS-degradable protecting groups or encapsulated within ROS-susceptible polymeric scaffolds for release in ROS-rich environments.^{26,132} Utilizing these degradative mechanisms, incorporation of ROS-susceptible functional groups and peptides into biomaterial platforms has led to substantial progress in ROS detection. Select examples of the chemistries of these macromolecular sensors are provided here, emphasizing that signal amplification, sensitivity, selectivity and specificity can be leveraged through bulk material properties.

In FRET-based systems, detection mechanisms are often linked to the de-quenching of a fluorophore or the efficient FRET between the

donor and acceptor moieties. For signal amplification, various donor/acceptor configurations and choices of material are possible.^{55,59,78,80,103,105} Weinstain *et al.* exploited electrostatic interaction of a fluorescently labeled polycationic cell-penetrating peptide (CPP) and a polyanionic peptide in a hairpin structure bound by an H₂O₂-susceptible linker.⁵⁵ Oxidation of the boronic acid-containing linker leads to fragmentation of the intact CPP such that separation of the donor and acceptor moieties causes FRET disruption (**Figure 3A**). Their probes exhibited selectivity towards H₂O₂ and high sensitivity (**Figure 3B**), allowing for low micromolar levels of detection and quantification of H₂O₂ in HL-60 cells. Furthermore, their system preserved spatial resolution, and proved sensitive enough to react with endogenous levels of ROS in an *in vivo* model of lung inflammation as visualized through fluorescence imaging (**Figure 3C**).

Although peptide-based FRET systems serve as powerful, non-invasive techniques to visualize endogenous ROS biology, limitations still exist in their photo-bleaching, stability within the local environment, low-depth tissue penetration of UV wavelengths, and auto-fluorescence from living tissue.^{22,133,134} In light of these issues, conjugating ROS-sensitive substrates to metallic nanoparticle donors may impart chemical and physical robustness. Metallic nanoparticles are especially attractive for their quenching efficiency, unique optical properties, biostability, ability to deliver non-membrane permeable components into the cell, and compatibility with multiple imaging platforms, all of which translates to improved performance *in vivo*.¹³⁵ Additionally, they can be functionalized with a variety of labeling molecules, leading to a wide range of possible biomolecular sensing constructs.⁴⁸ For example, in a recent study, Deepagan *et al.* used a PEGylated gold nanoparticle (AuNP) bearing fluorescein dyes and an H₂O₂-sensitive diselenide linker for ROS detection in activated macrophage cells.⁵⁹ Exposure of the nanoprobe to a H₂O₂-rich environment enabled fluorophore release upon diselenide bond cleavage. This probe improved over previously developed nanoprobos as a result of the diselenide bonds' enhanced hydrolytic stability under physiological conditions, and sufficient sensitivity towards physiologically relevant levels of ROS (50 μM). Other synthetic strategies utilizing a variety of non-toxic cores with optimal optical properties¹³⁶ are constantly emerging, such as carbon dots,¹⁰³ quantum dots (QDs),^{121,137,138} and metal nanoclusters.^{120,139} Similarly, additional resonance energy transfer processes have been explored to enhance sensitivity for *in vivo* imaging applications. For example, upconversion nanoparticles (UCNPs),^{78,84} which convert near infrared radiation (NIR) to visible light have proven beneficial in biosensing applications due to their ability to operate in the NIR region, avoid auto-fluorescence and enhance penetration depth.¹⁴⁰

To further leverage biomolecule functionality, hybrid approaches incorporating synthetic nanomaterials and chemical modification of biomolecules have also been proposed.^{141–144} In one example, Jiang *et al.* combined a chemically-modified green fluorescent protein (GFP) with a galactose-functionalized Au nanoparticle (AuNP-Gal) to

yield a platform with high stability and synergistic functionality for endogenous H₂O₂ detection in live cells (**Figure 4A**).⁵² By modifying the GFP lysines with various amounts of a boronate functionality, protein/AuNP-Gal complexes were formed through boronate ester formation (**Figure 4B**), which quenched GFP fluorescence. Subsequent incubation with H₂O₂ caused the complex to irreversibly dissociate as a result of bio-orthogonal oxidation of the boronate functionalities. This degradative process resulted in restoration of fluorescence (**Figure 4D**) as the phenylboronate (PB)-GFP and AuNP-Gal separate. Interestingly, the “ON”/“OFF” H₂O₂ sensitivity of their system could be fine-tuned by altering the ratio of boronate functionalities conjugated to GFP (**Figure 4C**). To test their system *in vitro*, they incubated their GFP functionalized AuNPs with human T lymphocyte Jurkat cells, successfully demonstrating *in situ* cellular oxidative stress monitoring. Thus, these hybrid strategies can leverage the unique physical and structural attributes of synthetic nanomaterials with the multi-site functionality of biological materials.

The majority of aforementioned systems use a single fluorescent intensity as the sensing signal, which may be hindered by variations in excitation intensity, inhomogeneous cell distribution, or probe concentration.¹⁴⁵ Additionally, they often lack the necessary spatial resolution to accurately track and monitor ROS in small volumes of cells, limiting their applications *in vivo*. In recent years, several strategies to overcome these limitations have been developed. For one, ratiometric approaches have become a common strategy to enhance sensitivity by affording simultaneous recording of two measurable signals in the presence and absence of their analyte without backscattering effects, a common by-product of fluorescence imaging. Additionally, by employing a reference signal, ratiometric sensors have a “built-in” self-calibration, which translates to higher levels of accuracy in terms of quantitative analysis.¹⁴⁶ Several nanoparticle biosensor platform systems using a combined FRET/ratiometric approach for ROS detection *in vitro*^{105–107,121} and imaging *in vivo*¹⁰³ of endogenous ROS have been developed. Going one step further, PA imaging modalities have also emerged to improve spatial and temporal resolution^{147,148} through the use of exogenous contrast agents, such as AuNPs.¹⁴⁹

While this section focuses on degradation as the material response, consideration of degradative susceptibility has been demonstrated as a key design criterion for stability in ROS-targeted platforms. For example, Dhada *et al.* created a PA contrast agent using a Au nanorod (AuNR) core with a shell consisting of poly-D-lysine (PDL) coupled to a ROS-sensitive near infrared dye, IR775c, (**Figure 5A**) for tracking mesenchymal stem cell viability in diseased environments (**Figure 5D**).⁶⁸ In this system, PDL was chosen based on known enzymatic resistance,⁶⁹ while the ROS-sensitive dye coupled with AuNRs as a secondary signal enabled highly sensitive visualization of the analyte through ratiometric detection (**Figure 5B**). Specifically, the probe's PA signal exhibits a broad peak at 780–800 nm and a small peak at 910 nm coinciding with IR775c and the AuNR, respectively. The

addition of ROS lead to a decrease in the IR775c PA signal while the AuNR PA signal did not change (**Figure 5C**). Their ratiometric system allowed for longitudinal, *in vivo* tracking of cell viability with high spatial and temporal resolution.

Many systems have also leveraged oxidatively induced molecular degradation to cause the bulk disassembly of a biomaterial platform, resulting in the release of fluorescent dyes as an indirect measure of ROS.^{10,11,14,150} In these cases, arylboronic esters are again the most commonly employed ROS-responsive units for detection of oxidative species with high sensitivity.^{16,150} For example, De Gracia Lux *et al.* developed boronic ester-containing polymeric nanoparticles capable of undergoing H₂O₂-induced backbone degradation, resulting in release of small molecule fluorescent imaging agents.⁵³ Advantages of this specific system are the fast cleavage kinetics, tunable polymer structure and good sensitivity (50-100 μM H₂O₂). Alternatively, Muhammad *et al.* exploited the oxidant susceptibility of thiol groups for an inflammation-triggered drug/imaging agent release system specifically responsive to •OH only.⁷⁰ In this system, the nanochannels of mesoporous silica nanoparticles were loaded with camptothecin, and then subsequently capped with thiol-stabilized zinc sulfide (ZnS) QDs. Upon oxidation of the thiol group, destabilization of the ZnS 'nanolids' leads to disassembly and release of the loaded contents, enabling detection of ROS at inflammatory sites with confocal imaging. In another follow-up study, they extend this strategy to oxidant-prone silver 'nanocaps', demonstrating utility to a variety of nanomaterials for ROS detection based on degradative processes.^{73,74}

Despite the usefulness of these types of oxidation-induced disassembling release systems, it is often difficult to deliver imaging agents to diseased tissue in a specific and controlled manner. To improve on these limitations for optimal clinical translation, materials that degrade only in response to combined stimuli ("AND" logic gates) could help improve accuracy, enhance effectiveness, and ultimately lead to targeted imaging specific to diseased conditions.¹⁵¹ Several small molecule fluorescent probes based on molecular logic gates have been constructed for ROS detection. For example, Sedgwick *et al.* recently developed a novel probe for simultaneous evaluation of ONOO⁻ and glutathione (GSH), two closely related inflammatory markers.¹⁵² Based on this groundwork, similar, synergistic approaches have begun to be incorporated into macromolecular sensors.^{57,83} For example, Mahmoud *et al.* developed a dual-response strategy with a polymeric nanoparticle that degrades upon exposure to two inflammatory disease biomarkers stimuli (acidic pH and elevated levels of H₂O₂) in tandem.⁷⁶ Their system is based on sequential chemical transformations: first, backbone thioether oxidation by ROS, which leads to greater solvation of the polymer, and second, acid-catalyzed cleavage of backbone ketal groups. In a similar fashion, Viger *et al.* designed dextran-based polymeric nanoparticles for detection of the same two stimuli (low pH and ROS).⁵⁶ In their design, dextran was rendered pH-sensitive by functionalization with acetal groups, and a

separate batch of dextran was rendered oxidation-sensitive by functionalization with arylboronic esters. Both responsive polymers were combined in nanoparticles loaded with a NIR dye. This dual-functionalization enabled the fluorescent probe to selectively turn "ON" in acidic and oxidative environments through release of the dye (**Figure 6A-C**). By using a combination of triggers, they achieve a variety of tunable material responses as dictated by environmental conditions (**Figure 6F**). By further modulating the material's interaction through variation in the biological targets, their nanoprobe demonstrates control over the speed, sensitivity and selectivity of signal activation (**Figure 6D, E**).

Combining materials responsive to complementary biomarkers (*e.g.*, low pH and increased levels of ROS), allows for detection of inflammatory conditions with enhanced sensitivity over systems responsive to only one biomarker. Furthermore, integrating a variety of responsive units into a single platform demonstrates the distinct advantages of taking a multifaceted approach to achieve a desired response. As the field of stimuli-responsive systems continues to grow, new design strategies leveraging the oxidatively degradable materials chemistries discussed here will pave the path to creating highly tunable platforms with enhanced sensing capabilities in inflammatory contexts with numerous closely tied biomarkers.

2.3 Sensing Based on Supramolecular Assembled Materials:

As described in the examples already presented here, and more extensively in a recent review by Stubelius *et al.*,¹⁶ the chemistry of boronic acids render extensive versatility for use in a wide range of biological applications. Beyond their use for ROS-triggered polymer degradation, oxidatively activated supramolecular assembly has also been achieved by incorporating boronic esters into polymers. Although the inherently dynamic nature of these types of systems compromise some level of selectivity towards single species, their reversible nature may enable the monitoring of dynamic enzymatic and oxidative pathways, warranting them valuable tools for further development in biosensing applications. For example, Huang *et al.* developed a redox self-assembly system designed to fluoresce only above a certain concentration of oxidant, facilitating detection of pathogenic threshold levels of ROS.⁸⁵ Their system leveraged an H₂O₂-activatable fluorogenic quinazolinone derivative (BQA) capped with an arylboronate immolative linker on a tetra peptide chain. Upon oxidation of the BQA, a phenyl group is exposed, which forms an intramolecular hydrogen bond and causes planarization of the molecule. The planarization then facilitates intermolecular π-π stacking and self-assembly (**Figure 7A**). The novelty of this system lies in the fluorescence dependence on the critical assembly concentration (CAC), tunable with the short peptide sequence (**Figure 7B**). They successfully used their system to show highly fluorescent assemblies inside malignant cells (Hep G2, MCF-7, and PANC-1) but not in corresponding normal cells (L-O2, MCF-10A and HUVEC), as validated with ROS inhibitors and inducers (**Figure 7C**). Because ROS exists in all living biological environments in some

capacity, differentiating basal and pathogenic levels of ROS is an important challenge in ROS sensing— especially in diseased contexts in which ROS concentrations are significantly increased to start. Therefore, the capability to not only detect ROS, but also report the threshold at which ROS becomes pathogenic, could be more informative for disease diagnostics.

2.4 Detection Based on Nanomaterial Interactions

While the above mentioned systems focus on a variety of oxidation reactions which result in material degradation and supramolecular assembly, targeted oxidation reactions can also be leveraged to mediate changes in nanomaterial interactions to produce a clear spectral shift. Although a limited number of systems in oxidative sensing have employed this approach, the chemistries employed are unique additions to the toolbox of materials provided in Table 1. For example, illustrating the functional diversity of sulfur-containing groups, cysteines can be transformed to cystines through iodide (I^-) catalyzed oxidation. As demonstrated by Wang *et al.*, this approach can be used to indirectly monitor glucose oxidation through downstream changes in AuNP interactions (**Figure 8A**). Specifically, simple oxidation-induced disruption of cysteine-capped AuNP aggregates (**Figure 8D-G**) result in detectable absorbance shifts (**Figure 8B-C**).⁸⁶ Furthermore, they illustrate the ability to use this colorimetric sensor to probe closely tied oxidative and enzymatic mechanisms. They implemented their detection platform to analyze H_2O_2 generation associated with the acetylcholine esterase/choline oxidase (AChE/ChOx) cascade, thereby validating the incorporation of simple chemistries into sensing platforms for analysis of more complex biological processes.

In another unique approach to utilizing nanomaterial interactions for ROS sensing, Gao and colleagues designed H_2O_2 nanosensors using a DNA competitive binding approach.⁸⁸ In their system, competitive coordination of cerium oxide nanowires with tagged, single-stranded (ss) DNA led to a fluorescent signal upon H_2O_2 displacement of adsorbed DNA from the nanowire surface. The binding occurs rapidly, enabling real-time monitoring of H_2O_2 fluctuations in RAW 264.7 macrophage cells. The fast response and high sensitivity was also demonstrated *in vivo*, leading to successful mapping of inflammation in wound-induced oxidative damage in zebrafish larvae.

2.5 Oxidatively Triggered Materials: Detection Based on Conformational Changes

Similar to the development of oxidatively triggered systems for ROS detection based on the degradation of materials, systems that rely on material conformational changes for detection also utilize reactions with ROS-susceptible functional groups. These groups include: L-cysteine, selenium, tellurium, ferrocene and polythioketals, among others. By incorporating these moieties into biomaterial platforms in contexts that lead to bond formation,

transfer, or rearrangement upon addition of oxidative stimuli, a variety of conformational changes in materials can be achieved. For example, oxidation of surface exposed cysteines within proteins can result in disulfide bond formation. This mechanism has been exploited in the well-known, commercially available HyPer probes. Beyond cysteine functionalities, other less-reactive sulfur-containing groups, such as the thioethers, are commonly exploited in poly(propylene sulfide) (PPS) based systems which undergo hydrophobic to -philic transitions in ROS rich environments.^{93,94} These reactions are based on oxidation of hydrophobic sulfides to hydrophilic sulfone or sulfoxides resulting in material swelling and cargo release.¹⁵³ Here, we focus on a select few of these cases to highlight how molecular changes in chemistry can be translated to large macromolecular conformational material responses for ROS detection.

Oxidatively triggered systems that undergo a change in hydrophobicity include sulfide,^{93,94} tellurium,^{99,102} ferrocene,^{100,101} and selenium⁹⁸ linked polymers. On the micro-scale, these groups react with ROS to add double-bonded oxygen atoms onto the chain, thus increasing overall hydrophilicity of the material. When incorporated into the main chain or side chains of hydrophobic and -philic polymer blocks, the resulting amphiphilic systems takes on a “solubility switch” mechanism that can be leveraged to release drugs and imaging agents as a result of swelling of the material. This was demonstrated by Allen *et al.* in which PPS particles undergo swelling and release cargo upon ROS stimulation.⁹³ Notably, their system responded to enzymatically driven H_2O_2 generation, thereby providing insight to upstream chloroperoxidase (CPO) and myeloperoxidase (MPO) enzyme activity. In another approach utilizing oxidation-induced hydrophobic to -philic transitions, Qiao *et al.* developed a unique polymer-peptide nanoparticle system for *in situ* treatment evaluation of a cytotoxic peptide.⁹⁴ Their system enabled ROS monitoring onset by poly(β -thioester) backbone oxidation. Specifically, transformation of the thioether bond to hydrophilic sulfoxides and sulfones lead to swelling and release of a “built in” PA imaging agent reporter, which subsequently formed H-aggregates in solution for enhanced signal.

It should also be noted that the ROS-responsive degradation properties of the boronic esters, discussed in 2.2, can be transduced into a solubility switch mechanism when integrated into block copolymers. This was demonstrated by Chen *et al.*, in which boronic acid groups were incorporated into a cross-linked polymer such that unmasking of the boronic esters upon oxidation transformed the group into a hydrophilic alcohol, leading to swelling of the material.¹¹⁶ Detection was attained through the use of a dual-colored ratiometric fluorophore, whose emission is highly sensitive to the surrounding environment. Upon swelling of the material, increasing polarity within the polymer nanoprobe lead to a green-to-blue ratiometric fluorescent transition. This example contrasts that previously demonstrated by Viger *et al.* with modified hydrophobic dextran particles,⁵⁶ in which full degradation and disassembly of the

backbone occurred upon oxidation. Essentially, these two examples illustrate the versatility conferred through the incorporation of boronic acids into materials in different fashions, demonstrating the ability to transduce the degradation properties of boronic esters into a larger scale material response.

Since their discovery nearly two decades ago, the field of genetically encoded fluorescent proteins has drastically expanded. Their ability to measure dynamic signal transduction pathways in living cells in a highly sensitive and spatiotemporal fashion has enabled a diverse array of biosensor designs for use in a wide range of applications. To best illustrate the breadth of this field, we direct the reader to an extensive review by Greenwald *et al.*,¹⁵⁴ which provides a comprehensive list of published genetically engineered fluorescent biosensors. Here, we turn to a subset of these sensors: the well-developed and commercially available HyPer probes. These systems are traditionally based on redox-sensitive variants of green fluorescent protein (GFP), which undergo intramolecular disulfide bond formation that directly leads to conformational rearrangements. In turn, alterations in protein conformation result in spectral changes. Rather than providing a complete account on this extensive subject, we will highlight only outstanding and recent design strategies of HyPer systems for *in vivo* applications, as digested in a recent review by Bilan *et al.*⁹²

HyPer probes enable spatiotemporal information at high resolution as a result of their ability to be localized within a biological environment (*e.g.*, cellular compartments or tissues of living organism).⁹² This property has contributed to their popularity for investigating the pathological and physiological function of H₂O₂ in a wide variety of *in vivo* models. HyPer probes are chimeric proteins comprised of two functional domains: OxyR (the regulatory domain of *E. Coli* transcription factor) linked via peptides to a fluorescent protein. The most frequently employed probes are grouped into three families represented by five variants: three circularly permuted yellow fluorescent proteins (cpYFP, HyPer1,2,3), one based on red fluorescent proteins (HyPer Red) and one based on redox sensitive GFP (roGFP) fused with yeast thiol peroxidase (Orp1) (**Figure 9A-C**).⁹¹ These systems are characterized by two fluorescence peaks, with unique ratiometric advantages resulting from peak intensity increasing proportionally with oxidation. Improved versions have expanded the dynamic range of H₂O₂ detection by introducing point mutations into the OxyR activating regulon domain, exemplifying the ability to alter the properties of proteins using single amino acid substitutions.^{155,156} The success of HyPer probes is also due to their compatibility with various imaging modalities, such as confocal microscopy, two-photon excitation, and fluorescent lifetime imaging (FLIM) microscopy. Because the fluorescence of most versions of HyPer are excited at two separate peaks, HyPer probes can yield ratiometric, dynamic and quantitative readouts that do not depend on protein expression levels in different cells.

Despite success *in vivo*, HyPer probes still suffer from several limitations. As a result of their biologic nature, these probes are often highly unstable and susceptible to other biological species. For example, high intracellular thiol-oxidizing environments can cause HyPer probes to become completely oxidized, which leads to confounding signals in sensing applications. Additionally, all HyPer probes are highly sensitive to pH changes in the physiological range. In light of these limitations, new strategies have emerged to improve sensing capabilities by combining the features of HyPer with other chemical functionalities, thereby allowing HyPer based probes to sense more than one parameter. For example, Mishina *et al.* fused HyPer with the pH domain of a tyrosine kinase to create a genetically encoded probe for sensing both H₂O₂ and phosphatidylinositol 3,4,5-triphosphate (PIP3), which indirectly reflects activity of phosphatidylinositol 3-kinase.⁴⁰ The probe's efficacy was demonstrated in fibroblasts, in which both H₂O₂ and PIP3 levels were successfully visualized, demonstrating the ability to develop biosensors with combined functionalities. In another example, Tao and colleagues demonstrated that H₂O₂ could be precisely quantified in the wound region of a zebrafish larval tail fin (a common model for inflammation).¹⁵⁷ For this system, they used a HyPer-Red probe in combination with a green fluorescent protein biosensor to create a multi-parameter system which enabled the simultaneous imaging of H₂O₂ and NADPH oxidase in real time. As illustrated by these examples, engineering biological functionality into sensing systems holds promise in the development of materials that seamlessly assimilate into the complex inflammatory milieu.

In summary, identification of oxidatively susceptible moieties has translated to a number of efficacious systems for applications in drug delivery and biosensing. However, off-target activation and low sensitivity levels continue to hinder optimal clinical translation. Furthermore, consideration of closely tied mechanisms, such as enzymatic inflammatory biomarkers, are often overlooked in biosensor design. By highlighting the common materials chemistries strategies utilized to detect and treat ROS-related disease, along with the advantages associated with differing types of material responses, we hope to provide a picture of ways to build upon these current limitations as we work towards integrated biosensors designed to capture the full spectrum of oxidative and enzymatic inflammatory pathways.

3 Applications and Discussion: Enzymatically Triggered Materials

3.1 Targeting Inflammatory enzymes

Enzymes dictate a wide range of biochemical reactions. Because their expression and activity are tightly linked to their local environment, they are optimal targets for biosensing applications.²³ Within the inflammatory environment, several classes of enzymes exist, including proteases (serine, cysteine, metallo, etc.), protein kinases (protein tyrosine/serine kinases) and protein phosphatases (protein

serine/threonine phosphatases). Imbalances or dysregulation of these enzymes often occur in inflammatory states, establishing them as informative biomarkers of disease progression.³⁶ Several materials have been developed to sense enzymatic activity (**Table 2**). Recalling Figure 2, these systems primarily fall into three of the four material response categories: degradative processes, supramolecular assembly/disassembly, and nanomaterial interactions. These changes are largely initiated by enzymatic interaction with specific peptide substrates. As a result, the biggest hurdle in designing sensors that achieve accurate detection and avoid signal convolution lies in overcoming substantial overlap in peptide substrate specificity.^{4,158–160} This challenge arises from the complex, cascading operations in enzyme activation and regulation in biological contexts. Thus, a better understanding of individual protease activity, as well as their interplay with numerous other species such as ROS, is necessary to successfully exploit enzymatic biomarkers for inflammatory disease detection. In an effort to identify what has been done in this field, this section will provide a digest of current strategies to achieve accurate enzymatic molecular recognition in inflammatory settings.

3.2 Enzymatically Triggered Materials: Detection based on Degradative Processes

Enzymes play a significant role in extracellular matrix turnover and tissue remodeling, making them especially attractive targets for biosensors based on degradative processes. Similar to oxidatively triggered materials in this realm, most systems employ fluorescence methods of detection. In particular, a common mechanism is the site-specific proteolytic cleavage of a peptidic scaffold resulting in fluorescence increase of the reporter molecule. To enhance sensor sensitivity beyond this single cleavage event, several systems combine the high quenching efficiency of AuNPs with the specific recognition properties of peptide substrates.^{6,69,80,161–164} In one example, Park *et al.* developed an AuNP FRET-based system for the detection of MMP-7 wherein carboxy AuNPs were tethered to a labeled, sequence-defined peptide via the coordination of Ni(II) metal ions.¹⁶⁵ Upon MMP-7 addition, significant fluorescent recovery was observed with a detection limit of 10 ng/mL. In a similar approach, Lee *et al.* used a AuNP with a near infrared fluorescence (NIRF) Cy5.5 probe conjugated to an MMP-specific peptide. Their system exploited the increased tissue penetration of NIR fluorescent imaging to visualize MMP-2 activity in tumor-bearing mice.¹⁶² A third example further optimizes NIR fluorescent AuNP probes using a combinatorial approach. Mu *et al.* synthesized libraries of AuNP probes with various surface compositions of self-assembled heterogeneous monolayers of dye-labeled peptides and PEG (**Figure 10A–B**).¹⁶⁶ Functional screens of trypsin and urokinase-type plasminogen activator (uPA) led to several trends for design criteria of the probes, as well as extended circulation time *in vivo*, as validated with NIR imaging of a tumor phantom model in an immunodeficient mouse (**Figure 10C–D**). Future research building on this combinatorial synthesis strategy could lead to multiplexed

systems for detection of numerous species in intricate inflammatory environments.

Beyond AuNPs, sensing with other nanoparticle platforms is another common method for enhancing detection sensitivity. Wang *et al.* used a FRET sensor employing two nanoparticles, upconversion phosphors (UCPs) and carbon nanoparticles (CNPs), as energy donor and acceptor pairs.¹⁶⁷ Their system was composed of a polypeptide chain comprising the MMP-2 substrate domain and a π -rich motif to the surface of UCPs. The FRET process was initiated by the π - π interaction between the peptide and carbon nanoparticles. Upon proteolytic cleavage of the substrate by the protease, the donor was separated from the acceptor thus restoring fluorescence. Owing to the hypersensitivity of this method, only 1 μ L of clinical samples were needed for accurate quantification. In another two particle approach, Shi *et al.* developed a hybrid nanomaterial consisting of an encapsulated silica nanoparticle as energy donor and AuNPs as energy acceptors linked by a caspase cleavable substrate.¹⁶⁸ Their peptide-bridged hybrid system allowed for ratiometric sensing of caspase-3 upon enzymatic triggered cleavage, increasing sensitivity (limit of detection \sim 6 pM), while also imparting selectivity over a variety of other species through their “satellite”-shaped hybrid structure.

While silica nanoparticles have risen as a promising tools in developing multifunctional nanomaterials in recent years,¹⁶⁹ other innovative nanomaterial structures offer additional strategies for improving probe characteristics. These include Au nanoclusters functionalized with MMP-cleavable linkers,¹⁷⁰ Au nanocages with surface plasmon resonance peaks well separated from the emission peak of the dye,¹⁷¹ QDs,^{172–175} UCNPs,^{167,176} and metal organic frameworks (MOFs).^{177–180}

ARTICLE

Table 2: Enzymatically Triggered Biomaterials

Responsive Component	Trigger**	Macromolecular Signal/Method of Detection++	Sensitivity (lowest reported detection)
Detection Based on Degradative Processes			
MMP cleavable peptide substrate	MMP-2,3,7,9,13, collagenase IV	Fluorescence, Luminescence, SPR, Chromatography	50 ng/mL ¹⁶³ ; 0.72 ng/mL ¹⁷¹ ; 5 nM ¹⁸¹ ; [250 ng/μL] ¹⁶¹ ; 50 nM ¹⁸² ; 25 ng/mL ⁸⁰ ; 10 ng/mL ¹⁶⁵ ; 2 ng/mL ¹⁷⁵ ; 1 nM ¹⁶² ; 10 pg/mL ¹⁶⁷ ; N/A ¹⁸³ ; 10 U/mL ¹⁸⁴ ; 0.52 ng/mL ^{185#} ; 0.15 nM ¹⁷⁰ ; 0.1 ng/mL ¹⁷⁹
Caspase cleavable peptide substrate	Caspase-1,3,8,9	Fluorescence, Luminescence	5-40 nM ¹⁸⁶ ; 6 pM ¹⁶⁸ ; 20 pM ^{172#} ; 1 nM ¹⁶⁴ ; 15 U ¹⁸³ ; 0.1-5 U/mL ¹⁸⁷ ; 0.6 nM ¹⁸⁸ ; 0.12 ng/mL ¹⁸⁰
Cathepsin cleavable peptide substrate	Cathepsin-K, B, L	Fluorescence, Luminescence	250 pM/mL ¹⁸⁹ ; 0.1-5 μg/mL ¹⁸⁷ ; 0.001 U/mL ¹⁷⁷ ; 2.5 U/mL ¹⁷⁸ ; 0.027 U/L ¹⁹⁰ ; 3.2 ng/mL ¹⁹¹
Serine protease cleavable peptide substrate	Trypsin, chymotrypsin	Fluorescence, Luminescence	2.5 mg/mL ¹⁹² ; 250 U ¹⁶⁶ ; N/A ¹⁸³ ; 0.2 μg/mL ¹⁹³
Peptide triple-helical substrates	MMP-2,9	Fluorescence	5 nM ¹⁹⁴
Genetically encoded fluorescent proteins	MMP-9, Caspase-1	Fluorescence, Luminescence	10 μg/mL ¹⁹⁵ ; N/A ¹⁹⁶
Peptoid based substrates	MMP-13 and MMP-14/MT1-MMP, Cathepsin-G	Chromatography, Fluorescence	20 nM ¹⁹⁷ ; 10 nM ¹⁹⁸
Poly-L-Lysine	Trypsin	Fluorescence	2.5 mg/mL ^{199;69}
Hyaluronic Acid	Hyaluronidase	Fluorescence	0.1 U/mL ²⁰⁰ ; 0.6 ng/mL ¹⁷⁶
Detection Based on Supramolecular Assembly/Disassembly			
MMP cleavable peptide substrate	MMP-2,9	Chromatography, Fluorescence, Nanoparticle size	1 μg/mL ²⁰¹ ; 100 ng/mL ²⁰² ; 10 nM ²⁰³ ; [MMP-2: ~50 U/L; MMP-9: ~80 U/L] ²⁰⁴

Journal Name

ARTICLE

Caspase cleavable DEVD peptide substrate	Caspase-3,7	Chromatography, Fluorescence, Nanoparticle size	1 pM ²⁰⁵ ; 0.0049 U/mL ²⁰⁶
Serine, tyrosine-containing substrates	Protein Kinase A (PKA), Protein Phosphatase-1 (PP1), PKC α	Fluorescence, Nanoparticle size	[PKA: 5 ug/mL + 2 mM ATP; PP1: 0.8 ug/mL + 1 mM MnCl ₂] ^{204*} ; 0.05 U/mL ²⁰⁷ ; [0.1 U/ μ L PKA or 1.1 ng/ μ L PKC α] ²⁰⁸
Phosphoanhydride bonds	Alkaline Phosphatase	Chromatography, Nanoparticle size, Fluorescence	150 U/L ²⁰⁹
Hyaluronic Acid	Hyaluronidase	Fluorescence, SPR, Nanoparticle size	0.02 U/mL ²¹⁰ ; 1 U/mL ^{211#} ; 0.0017 U/mL ^{212#}
Detection Based on Nanomaterial Interactions			
MMP susceptible substrates	MMP-2,7,9	MRI, SPR, Nanoparticle size, Fluorescence	6.5 U/mL ²¹³ ; 2 μ g/mL ²¹⁴ ; 3 nM ²¹⁵ ; 221 U/mL ²¹⁶ ; 100 ng/mL ²¹⁷ ; 10 pM ²¹⁸
Caspase Cleavable DEVD Peptide Substrate	Caspase-3	SPR	0.005 μ g/mL ²¹⁹
Cathepsin cleavable peptide substrate	Cathepsin-L	SPR	16 ng/mL ¹⁹¹
Threonine, tyrosine, and serine-containing substrates	PTP/Abl Kinase, ALP, PKA, Src Kinase, Her2 Kinase, Trypsin, chymotrypsin	MRI, SPR, Nanoparticle size, Fluorescence	[4 U/ μ L PTP; 0.5-2.5 U/ μ L Abl kinase] ^{220*} ; 0.01 U/mL ²²¹ ; 50 U/mL ²²² , 5 nM ²²³ ; 7.5 nM ¹⁷³ ; 0.032 U/mL ²²⁴ ; 250 U/mL ²²⁵ ; [85 nM trypsin or 170 μ M chymotrypsin] ²²⁶ ; 0.01 U/mL ²²⁷

#indicates ratiometric, *indicates reversible

****Triggers Included [Enzyme class (subclasses)]:** [matrix metalloproteinases (MMP-1,2,3, 7, 8,9,13), membrane type 1 MMP (MT1-MMP)], [cysteine proteases (caspase 3,7,8, cathepsins K, G, B)]; [serine proteases (trypsin, chymotrypsin)]; [protein phosphatases (Protein Phosphatase-1, PP1), (protein tyrosine phosphatase, PTP), (Alkaline Phosphatase, ALP)]; [Protein Kinases A, (PKA), protein kinase C (PKC) Abelson tyrosine Kinase (Abl kinase), Src Kinase], hyaluronidase

++ Methods of Detection: Fluorescence (*e.g.*, fluorescence spectroscopy, imaging, FRET); Surface Plasmon Resonance (SPR) (*e.g.*, absorption spectroscopy, photoacoustic imaging); photoinduced electron transfer (PET); Luminescence (Chemi- or Bioluminescence); Nanoparticle size (analytical methods include Dynamic Light Scattering (DLS), electron microscopy, turbidity); Chromatography (*e.g.*, High Performance Liquid

ARTICLE

MOFs have become an increasingly attractive area in biosensing research in recent years for their ability to impart stability and retain biological activity.²²⁸ Most notably, nanoparticles linked to MOFs have been developed as a platform for a dual-recognition switch in sensing applications. Similar to the ROS systems that employed “AND” logic methodology discussed previously, nanoparticle MOF constructs can be used to detect intracellular enzyme activity in combination with pH changes. Shen *et al.* demonstrated this approach using a core-shell nanoparticle peptide MOF for stepwise-responsive recognition of cathepsin B in living cells, the first report of a bio-recognition switch embedded into a MOF for imaging in live cells.¹⁷⁸ Specifically, their system used a pH-sensitive shell and a AuNP core functionalized with a peptide substrate susceptible to cathepsin B to sequentially respond to acidic conditions and enzymatic activity of lysosomal cathepsin B, enabling highly localized and sensitive imaging inside HeLa cells.

Beyond nanoparticles, proteins have been utilized as energy donors to complement QD energy acceptors in a variety of ways. One innovative approach leveraged bioluminescence energy transfer (BRET). While FRET requires fluorescence initiation by an external source, which can cause background noise and photo-bleaching, BRET utilizes energy released by a chemical reaction in the form of light emission.^{229–231} Taking advantage of these characteristics, Yao *et al.* developed a BRET-based QD sensor for detection of MMPs.¹⁷⁵ In their system, a bioluminescent light-emitting protein, *Renilla* luciferase, served as the energy donor. Their ratiometric approach enabled detection of MMP-2 to levels as low as 5 ng/mL (~75 pM) and demonstrated selectivity over other members of the MMP family (MMP-7). In another protein-QD example, Boeneman *et al.* genetically modified a caspase-3 cleavage site into a fluorescent mCherry protein for conjugation to QDs, achieving sensitivities in the picomolar range (~20 pM).¹⁷²

Although the use of nanoparticle platforms dominate substrate-based FRET detection methods, systems using polymeric platforms have also found success. For example, Lee *et al.* developed a polymeric nanoparticle of poly(lactic-co-glycolic acid) (PLGA) and polyethylenimine (PEI) linked to an MMP-2 activated peptide sensor consisting of an NIR fluorescence dye and quencher (**Figure 11A–B**).¹⁸² Their system (MMP-2-PLGA-PEI) allowed for the continuous tracking and accurate detection of MMP-2 activity in “MMP-2-positive” cancer cells (HaCat cells) as compared to “MMP-2-negative” cells (MCF-7) (**Figure 11C**). Most notably, the particles showed high specificity for MMP-2 over MMP-1,3,7 and also substantial specificity over MMP-9 and 13 (**Figure 11D**). Analogous to Lee’s MMP-probe, copolymers for imaging cathepsins have also

been used. Jaffer *et al.* developed a NIRF imaging agent using a Cy5.5-labelled copolymer with a cathepsin susceptible peptide sequence.¹⁸⁹ This system showed high selectivity for cathepsin K and was used to monitor the activity of cathepsin K in mouse and human atherosclerosis models, eliciting high fluorescence signals in plaque sections. The probes demonstrated the ability to image enzymatic activity localized primarily in the vicinity of cathepsin K positive macrophages.

As presented thus far, most sensors are designed for detection of single species, making it difficult to reveal the interrelationship of biomarkers *in situ*. To improve understanding of the complex and cascading operations of enzymes within the inflammatory environment, sensors capable of detecting both upstream and downstream regulatory proteins in order to monitor their roles in biochemical pathways are needed. To sequentially visualize the evolution of cathepsin B and caspase-3, two important biomarkers of the apoptotic pathway, Gao *et al.* designed a AuNP probe with two fluorogenic peptide chains functionalized to the surface using a selenide bond.¹⁸⁷ Their design exhibited stability and anti-interference in MCF-7 cells, allowing real-time *in situ* monitoring of cathepsin B and caspase-3 activity. In an adjacent approach, Park *et al.* linked fluorescent protein-conjugated AuNPs for simultaneous detection of multiple caspase activities.¹⁸⁶ Using simple peptide substitutions and different colored fluorescent proteins, they were able to detect different types of caspases (both initiator caspases-8 and -9 as well as effector caspase-3) for real-time detection of the apoptotic pathway *in vitro*. Future development of sensors that can be used in complicated biological systems for investigation of intracellular enzyme interactions could greatly advance our understanding of mechanistic cellular behaviors dictating disease pathogenesis, which would ultimately translate to improving disease diagnosis.

As illustrated by the systems discussed here, the use of synthetic peptide substrates has resulted in a variety of efficacious sensing systems capable of detecting numerous proteases based on degradative processes relevant in inflammatory contexts. Although overlapping specificity issues and cross-reactivity remain a challenge, a variety of inorganic platforms have facilitated stability of these systems, while numerous synthetic strategies have been developed to add additional levels of tunability. Future development of these sensing systems based on degradative processes appear promising in the detection of cascading enzymatic activity present in inflammatory environments.

3.3 Enzymatically Triggered Materials: Detection Based on Supramolecular Assembly/Disassembly

Although efficacious, enzymatically-degradable substrates often serve as “one-time” sensors and are therefore limited in the information they provide. In light of this limitation, materials based on the enzymatically triggered supramolecular assembly and disassembly of molecules have been developed in an attempt to achieve dynamic detection.^{23,232} Supramolecular assembled materials are held together by non-covalent forces, enabling inherent flexibility and adaptability for sensing applications.^{233,234} This ability to dictate supramolecular material action through the systematic tuning of the underlying materials chemistries is important in the development of biosensors in which programmed responses are desired. We highlight a number of these systems here, which can be designed to control engagement and susceptibility to enzymatic action through a variety of techniques.

Many enzyme-responsive supramolecular materials rely on the self-assembly of peptide structures, which are known for their ability to partake in intermolecular interactions such as β -sheet formation and α -helical structures. Using rational design of peptide sequence, modular platforms with intracellular supramolecular organization have been achieved.^{203,206} In a unique approach for real-time tracking of drug release, Cheng *et al.* used an MMP-2 responsive prodrug that selectively cleaved into two parts: one containing a CPP linked to a therapeutic unit (doxorubicin, DOX), and the other containing a tetraphenylethene peptide derivative (PyTPE) that fluoresces upon self-aggregation (**Figure 12A**).²⁰³ Without MMP-2, the prodrug cannot efficiently enter the cells. Post MMP-2 cleavage, the therapeutic domain is freed to enter the cell via the CPP while the PyTPE self-aggregates due to hydrophobic interactions, resulting in yellow fluorescence and confirming intracellular release of the DOX therapeutic unit. The group was able to successfully demonstrate long-term tracking of anticancer drugs in HeLa cells, as well as detect variations in MMP-2 expression levels across different cell lines (**Figure 12B-E**). In another example, Ye *et al.* detected caspase-3/7 through the intracellular aggregation of fluorescent probes in tumor-bearing mice.²⁰⁶ Their probe contained a caspase-sensitive peptide, DEVD, which was cleaved in apoptotic tumor tissue, leading to intracellular uptake and intramolecular cyclization. Due to hydrophobic interactions between cyclized molecules, fluorescent nanoaggregates were formed with good retention at the apoptotic site and high fluorescent signal.

One of the most attractive features of enzymes as triggers is the fact that many of enzymatic reactions are reversible and thus can be exploited for reversible material changes. For this reason, exploiting enzyme pairs that catalyze complementary and reverse reactions—the phosphatase/kinase enzyme pair serving as the most prolific example—could find use in dynamically monitoring their complex and overlapping activity in inflammatory contexts. For example, Wang *et al.* prepared a doubly hydrophilic peptide-polymer system consisting of a PEG and polylysine block.²⁰⁹ When mixed with ATP,

electrostatic interactions allowed the ATP to attach to the lysines, creating a ‘superamphiphile’ that subsequently self-assembled into micelles. These structures could then be disassembled through introduction of phosphatase, restoring the polymers’ hydrophilic nature through hydrolysis of the ATP phosphoanhydride bonds. Despite advantages of dynamic systems such as these, only the phosphatase/kinase system has successfully accomplished reversible conformational changes in a material,^{204,220,235} and few have successfully been employed in sensing applications. Recognizing this research gap reiterates the call for a comprehensive approach towards development of next generation biosensors that exploit the intertwined activities of a wide range of inflammatory biomarkers.

3.4: Enzymatically Triggered Materials: Detection Based on Nanomaterial Interactions

Beyond peptide self-assembly, nanoparticle-based systems have also been used as a simple yet sensitive method in sensing and imaging applications.^{48,135,141,236–238} In contrast to degradative systems that characteristically utilize fluorescent methods of detection through cleavage of fluorogenic peptides linked to a nanoparticle, the method of detection in this category is based on colorimetric assays; namely, colloidal suspensions of NPs exhibit dispersion-dependent absorbance due to interparticle plasmon coupling, which can be used to provide a label-free, convenient readout for the detection of enzymatic activity.^{48,239} This is typically quantified by SPR shifts due to changes in interparticle spacing following enzymatic engagement. In these systems, two types of nanoparticle interactions are typically seen: (1) those based on aggregation due to physical, non-covalent mediated nanoparticle interactions (hydrophobic association and/or electrostatic interactions) and (2) those based on biochemical affinity between nanoparticles as a result of antibody,²²³ avidin-biotin,²²⁵ or DNA-mediated^{218,240} interactions.

Non-covalent aggregation based assays are attractive in that they take place rapidly because molecular recognition on the nanoparticle surface is not necessary.²²² For example, kinase was shown to dephosphorylate peptide substrates, leading to enhanced electrostatic interactions that facilitated adsorption onto AuNPs. Above a critical concentration, the adsorbed peptides induced AuNP aggregation, leading to a colorimetric change (Oishi *et al.*).²²² A similar approach using AuNRs was performed by Kitazaki *et al.*²²⁷ In another example of enzyme-mediated electrostatic interactions, Pan *et al.* designed a AuNP with a caspase-sensitive peptide substrate that released a positively charged fragment upon cleavage.²¹⁹ Upon binding of the positively charged fragment to the AuNP surface, the electrostatic stability of the AuNPs was disrupted, leading to aggregation and a color change related to caspase-3 activity. Although not in our discussion scope here, it should also be noted that the aggregation of iron oxide nanoparticles can be tuned with MMP-degradable coatings, leading to enzymatically-sensitive MRI imaging and detection.^{213,214}

Alternatively, affinity-based interactions between nanoparticles can also be mediated by metal chelators,²¹⁵ antibodies,^{174,223} or highly

specific binding pairs.²²⁶ While the metal binding affinity approach circumvents the need for antibody labeling, complex media contains salts and metal ions that may cross-react with the nanoparticle surface. Thus, nanoparticle interactions using highly specific antibodies or binding pairs such as streptavidin-biotin have had greater success in applications requiring efficient biochemical interaction with the analyte of interest. Strategies using these types of binding interactions to drive particle aggregation have been demonstrated for detection of kinases²²³ and MMPs.²¹⁶ In one study, kinase-catalyzed biotinylation of peptide-coated AuNPs was detected using complementary streptavidin-coated AuNPs. Upon the high affinity streptavidin-biotin interaction, the resulting particle aggregates led to a detectable colorimetric change of the suspension.^{225,241} However, these types of detection formats typically require a two-stage process, necessitating both surface modification of the nanoparticles with ligands as well as labeling of the analytes. Drawbacks of these cumbersome procedures limit *in vivo* translation. To circumvent these issues, Gupta *et al.* developed an alternative, single step approach in which two populations of AuNPs were used to detect kinase activity.²²³ Their system was based on simultaneous addition of kinase, unlabeled ATP and two particle types: one particle coated with a protein kinase substrate peptide and the other coated with complementary antiphosphotyrosine antibodies (**Figure 13A**). In a “one pot” approach, enzymatic phosphorylation of the peptides led to interparticle cross-linking due to specific recognition by the antibody-functionalized particles, which led to changes in absorbance intensity of the plasmon resonance peak (**Figure 13B**). Specificity and selectivity towards distinct targets of this type of system is especially high because the antibodies bind directly to the phosphate groups, thus minimizing the risk of off-target binding and confounding signals. Sensitivity is also high with detection levels in the nanomolar range, meeting requirements for *in vivo* diagnostic applications.

Nanoparticle interactions can also be mediated by enzymatically-triggered molecular recognition of nucleotide based systems. The most useful aspect of utilizing DNA in sensing applications is their inherent biocompatibility, stability and information storage capacity, which enables the possibility to encode information.^{144,242} Utilizing this approach, Kim *et al.* synthesized AuNP platforms functionalized with DNA-peptide molecules.²¹⁸ Upon MMP-2 cleavage of the peptide-DNA bond, the DNA diffused away from the NP to form a DNA-RNA heteroduplex on another set of AuNPs functionalized with fluorescently labeled RNA on the surface. Duplex formation lead to RNA digestion by RNase H, leading to fluorescence recovery upon liberation of the labeled RNA molecules. While diffusion dependence is less feasible in complex environments where interference with other biomolecules is likely, the advantage of this system is the high level of sensitivity as quantified by the low level of detection of 10 pM, thereby demonstrating the benefits of oligonucleotide duplex formation for signal amplification.

In summary, the versatility of enzymatically susceptible substrates has translated to a number of successful systems for applications in

biosensing. By highlighting the common approaches utilized to monitor and track enzymatic activity, we hope to further build upon the toolbox of materials chemistries presented in section 2. Together, we believe this repertoire of stimuli-responsive macromolecular materials will pave the path towards integrated, multi-responsive biosensors designed to cohesively capture the full spectrum of overlapping enzymatic and oxidative inflammatory pathways.

4: Multi-Responsive Systems with Wide Applicability

As the field of stimuli-responsive systems continues to grow, new design strategies will drive progress on creating highly tunable platforms with enhanced sensing capabilities in inflammatory contexts with numerous closely tied biomarkers. The ability to develop next-generation materials hinges on the ability to achieve sensitive responses in these complex biological environments. Despite the development of many enzymatically and oxidatively triggered sensing systems, they often suffer from non-specific activation owing to proteolytic cross reactivity¹⁵⁸ or ROS instability^{17,19} in inflammatory environments. Despite these limitations, much can be learned from the materials chemistry research progress in these fields, which poses the opportunity to exploit selective oxidative and enzymatic mechanisms to create multi-responsive materials. To date, a limited number of systems have been developed employing synergistic enzymatic and oxidative mechanisms in application. However, development of systems consisting of well-defined structural elements that specifically, accurately and sensitively respond to enzymatic and oxidative stimuli in a cooperative fashion could provide a route to systems capable of sensing specific patterns of multiple biochemical stimuli through programmed enzyme and oxidative-directed material responses. Here, we highlight a few select cases which provide an overview of progress in the field toward multi-responsive materials in the categories of degradative processes, supramolecular assembly and nanomaterial interactions.

4.1 Degradative Processes: Dual-Responsive Materials for Theranostic and Imaging Applications

Adapting a multi-responsive approach to exploit simultaneous and selective enzymatic and oxidative degradation, Han *et al.* used AuNPs covered by PEG chains with separate MMP-degradable *and* ROS-labile linkers (**Figure 14**).⁸⁰ Upon exposure to tumor tissue where MMP-2 is overexpressed, the MMP-degradable linker is cleaved, releasing a fluorophore to image the tumor. Meanwhile, the AuNPs are internalized by tumor cells, wherein the thioketal (TK) ROS-sensitive linker is degraded, releasing DOX to kill the tumor cells. To demonstrate the ability to differentiate tumor cells from healthy ones, the authors imaged their probe with squamous cell carcinoma cells (SCC-7) and normal kidney fibroblasts (COS7), and found that fluorescence recovery was more significantly observed in the cancerous cells. Furthermore, they demonstrated DOX release upon

light irradiation, which yielded antitumor therapeutic efficacy via growth inhibition of the SCC-7 cells. Other multifunctional systems exploiting thioketal chemistries and enzymatic and oxidative synergism for theranostic applications have also been explored.^{78,83,243} Yue *et al.* proposed a theranostic system based on pegylated UCNPs loaded with a photosensitizer and a chemotherapeutic drug for simultaneous optical imaging, photodynamic therapy and chemotherapy.⁷⁸ These results not only show promising potential for targeted, on-demand drug release and localized tumor imaging, but they also illustrate the value in taking a holistic approach to biomaterial design by exploiting synergistic oxidative and enzymatic effects for combined therapeutic and diagnostic goals.

4.2 Supramolecular Assembly: Linking Morphology to Different Enzyme Activities

Systems exploiting enzyme pairs that catalyze complementary and reversible reactions, such as the phosphatase/kinase pair, have found great utility in the controlled self-assembly and disassembly of materials for dynamic sensing applications. Employing a multiplexed approach, Ku *et al.* created a polymer-peptide amphiphile system leveraging sequence-specific peptides that take on distinct self-assembled morphologies following enzymatic interaction.²⁰⁴ Peptide substrates were selected for four different inflammatory associated analytes: protein kinase A (PKA), protein phosphatase-1 (PP1), MMP-2, and MMP-9. By incorporating these various enzyme substrates into the polar head groups of copolymers, the supramolecular assembly and disassembly could be modified by multiple enzymatic mechanisms: dephosphorylation by PP1 at serine residues, phosphorylation by PKA at serine residues, and/or peptide cleavage by MMPs at Gly-Leu peptide bonds. Depending on the enzymatic stimulus, several material responses were observed: larger amorphous aggregates, "network" aggregates or spherical micelles (**Figure 15**). Most notably, this system was able to selectively sense one analyte over another based on the final material response, demonstrating the ability to design enzymatically switchable micellar morphologies through simple sequence-specific incorporation of enzymatically susceptible peptides. To date, supramolecular materials including oxidative functionalities pale in comparison to endeavors in creating enzyme responsive supramolecular materials (discussed in section 3.2). To truly exploit the potential of supramolecularly assembled materials for accurate detection of inflammatory conditions, we must improve our understanding of the underlying chemistries dictating self-assembly processes, and also consider oxidative susceptible functionalities. Further development of dynamic supramolecular assembly systems, such as those discussed here, will provide valuable knowledge tools in sensing specific patterns of multiple biochemical stimuli through programmed enzyme and oxidative-directed material responses.

4.3 Nanomaterial Interactions: Applications in Multiplexed Detection

As we have mentioned, applications aimed to detect multiple enzymes have often led to complications such as substrate cross-reactivity, signal overlap and loss of sensitivity. However, these issues can often be addressed using systematic synthetic design.^{173,174} Lowe *et al.* demonstrated this in a unique multiplexing approach capable of differentially detecting enzymes from two classes, proteases and kinases, in complex environments.¹⁷³ Two different enzyme-specific peptide sequences were synthesized with orthogonal terminal functionalization for attachment to QDs with distinct emission spectra. One peptide substrate was cleavable by uPA, and the other peptide substrate contained a tyrosine for phosphorylation by the kinase activity of human epidermal growth factor receptor 2 (Her2). Upon simultaneous enzymatic activity, the addition of orthogonally functionalized QDs allowed for distinct changes in emission spectra (**Figure 16**). Specifically, the cleaved uPA peptide bound via streptavidin-biotin interaction led to de-quenching, while the phosphorylated peptide bound via His tag affinity led to FRET with labeled anti-phosphotyrosine antibody. The ability to accurately sense multiple analytes highlights the value in capitalizing on the specificity of biomolecular interactions based on antibodies and peptides, and further illustrates the value in taking a hybrid nanomaterial approach in biosensor design. Furthermore, the modular nature of this biosensor design is amenable for extension to different classes of enzymes.

A holistic consideration of the materials chemistries presented in this section illustrate that the ideas for the development of multifunctional biosensors are essentially limitless. With a plethora of synthetic strategies at our disposal, nearly any fluorescent protein, small molecule probe or fluorogenic peptide substrate can be combined with a variety of material platforms to impart unique sensing capabilities. In particular, leveraging key elements of biomolecular specificity with the optical and spectroscopic attributes of nanomaterials enables selective detection of specific enzymes, ROS, or multi-responsive behavior towards both.

5: Looking Forward to Advanced Biosensor Design

An overwhelming amount of approaches, even beyond those discussed here, have been employed to detect RNS/ROS and enzymes. However, the key challenge in achieving sensing systems that are selective, specific and sensitive enough to accurately and differentially detect ROS and enzymes stems from their complex and overlapping roles in diseased environments (**Figure 1A**). As a result, many systems still suffer from cross reactivity with off-target species, lack of specificity towards a single biomarker, *in vivo* instability, and insufficient detection limits. Research on stimuli-responsive biomaterials with tighter chemical control and connection between material response and analyte of interest is improving, and the integration of these materials into biological surroundings, such as inflammatory environments, for disease detection is increasing. This knowledge is complemented with increased understanding of the chemistry and biology dictating ROS/RNS and enzyme interactions, as well as evidence linking dysregulation of these species to distinct

pathological conditions. Additionally, the impact of synthetic design strategies, such as sequence-controlled materials, is an emerging research area that holds promise in the field of biosensing.²⁴⁴ In this section, we discuss some of the most pressing limitations of enzymatic and oxidative biosensors, as well as strategies for mitigation based on the toolbox of materials chemistries and design strategies discussed. By connecting these contributions comprehensively, future biosensors can be designed to seamlessly interact with their environments for improved accuracy in detection and monitoring of pathological conditions.

5.1 Avoiding Cross-Reactivity for Enhanced Selectivity

Achieving accurate detection of one species in complex biological environments where other oxidants and enzymatic species are present is a major challenge in biosensing.¹⁵⁸ Despite reported success of many systems, protecting against cross-reactivity is often overlooked in sensor design. For example, hyaluronic acid (HA) is susceptible to degradation by ROS, as well as hyaluronidase, another enzyme biomarker found in inflammatory environments. Despite this cross-reactivity, several HA-based probes for ROS and hyaluronidase have been developed. For example, Chen *et al.* developed an UCNP for highly sensitive bioimaging of ROS *in vitro*, as well as effective diagnosis of rheumatoid arthritis *in vivo*.⁸⁴ Their system utilized HA as a ligand to engineer UCNPs with luminescence energy transfer (LRET) detection. In this approach, multiple functional groups on the HA backbone enabled conjugation of upconversion luminescence (UCL) acceptor chromophores. The nanoprobe exhibited susceptibility towards various ROS and RNS ($\cdot\text{OH}$, $\text{ClO}\cdot$, $\text{ONOO}\cdot$ and $\text{O}_2\cdot^-$) with low detection limits (0.03, 0.02, 0.06 and 0.1 μM , respectively). Alternatively, Yang *et al.*²⁰⁰ and Wang *et al.*¹⁷⁶ developed carbon dot and UCNP based systems permitting sensitive detection of hyaluronidase through the digestion of HA, resulting in fluorescence recovery. It is clear that HA is susceptible to both ROS and enzymes in inflammatory contexts. This could lead to potentially confounding signals in application due to overlapping enzymatic and oxidative sensor susceptibility.

One intriguing approach to minimize cross-reactivity and improve sensor stability is the use of 'selectivity filters,' which employ a steric barrier that limits analyte diffusion or requires a user-designed precursor step that leads to sensor activation. Physical or steric barriers have been used to limit competitive peptide degradation by other enzyme species,²⁴⁵ but these barriers are most effective when screening out potential cross reactants based on size. A sensor developed by Kumar *et al.* demonstrates this best by entrapping a ROS-sensitive enzyme, horseradish peroxidase (HRP), within hollow Au 'nanoshells.' The pores of the metallic nanoshell are large enough to allow diffusion of ROS and small substrates for detection, yet they restrict access by molecules larger than 10 kDa.²⁴⁶ In addition to preventing degradative molecules from accessing HRP, the shell provides the added benefit of containing the HRP within the sensor for long-term localization. The second selectivity filter design implements a screening precursor step that can, for example, bind a

catalytic element, or expose a reactive substrate via stimuli-responsive degradation that activates the sensor. This strategy can be especially useful to localize a sensor to its target region of interest, as demonstrated by Cui and colleagues.²⁴⁷ They used an acid-sensitive PEG coating that localized their particle to sites of inflammation, which typically have a lower pH, before exposing its functional elements. Similar strategies can be used for selective sensing of ROS within acidified intracellular compartments and tumor cores. In another example, Rotello's group demonstrated that enzymatic substrate selectivity could be controlled using physicochemical properties of NPs, successfully using amino-acid-functionalized gold clusters to modulate the catalytic behavior of α -chymotrypsin towards cationic, neutral or anionic substrates.²⁴⁸ By balancing steric effects and electrostatic effects between the negatively-charged amino acid-containing NP monolayer and enzyme substrates, they observed repulsion of anionic substrates and increased specificity for cationic substrates.²⁴⁹

5.2 Improving Substrate Specificity

The use of protein substrates can limit the specificity and *in vivo* stability of sensors. In complex biological environments, opposing factors, such as pH and presence of ROS, can influence overall protein properties, such as charge state—which in turn can influence substrate-analyte interactions. Additionally, as proteolysis proceeds, protein substrates change, altering susceptibility that is difficult to control and monitor in sensing applications. Stability of these systems against hydrolysis in the bloodstream or cross-degradation of the substrate by off-target enzymatic species present in surrounding tissue can also diminish specificity, significantly affect the accuracy of detection. As a result, the use of synthetic, sequence-controlled peptide and peptoid substrates may be an attractive approach moving forward because their susceptibility is not necessarily dependent upon higher-order folded structure.²⁴⁴

Although synthetic peptides can be used to improve selectivity of systems against off-target degradation, developing systems with sufficient specificity within enzyme and ROS subclasses is also a significant challenge. For example, the gelatinases (MMP-2 and -9) are two closely related biomarkers associated with cancer cell invasion and cancer-related angiogenesis. However, expression levels of MMP-2 are often much higher than those of MMP-9, resulting in sensing signals reflecting proteolytic activity of MMP-2 rather than MMP-9, despite MMP-9 being a more informative prognostic marker in cancer.¹⁹⁵ Failure to link detection signals to distinct proteolytic species and their activity in pathological processes can severely limit diagnostic capabilities, yet most detection methods are based on substrates general to classes of enzymes and ROS, rather than distinct species. For example, Akers *et al.* developed a NIRF probe based on triple helical peptide substrates containing gelatinase sensitive sequences. Upon enzymatic cleavage, the peptide chains are released, resulting in amplified fluorescent signal.¹⁹⁴ Although their results proved suitable for *in vivo* detection

of general MMP activity, they could not differentiate between MMP-2 and MMP-9. Several other systems suffer from this same limitation.

When it comes to research improving substrate specificity profiling, substantial efforts revealing important trends and “consensus” sequences towards distinct subclasses of proteases have been made, but developing systems that achieve accurate and specific detection in application remains difficult.^{158–160,250} This results from the fact that the proteases are involved in numerous and overlapping intra- and inter-cellular inflammatory pathways, such that even well-established “consensus” peptide sequences often serve as good substrates for multiple species or specie subtypes. Progress towards improved specificity, as well as the continuous discovery of new “consensus” substrates, warrants an entire field in itself, and it is anticipated that sequence profiling will continue to improve.²⁵¹ However, these studies still expose an inherent limitation by employing purely natural substrates. Namely, there exists significant overlap and interchangeability between amino acid sequences, which hinders both substrate specificity and selectivity in complex biological environments.

To mitigate cross-reactivity issues, synthetic strategies have been employed. For example, it has been demonstrated that incorporating non-natural residues within peptide substrates could potentially lend bio-orthogonal functionality to consensus sequences, while significantly simplifying synthetic design requirements.^{197,198} For example, Stawikowski and colleagues designed triple helical substrates with select N-substitutions (peptoid residues) to evaluate helical stability and proteolysis of collagenolytic MMPs.¹⁹⁷ Their key finding was a substrate with two peptoid substitutions (synthetic peptidomimetics) that achieved specificity for MMP-13 over MMP-1 and MMP-8 at low detection limits (20 nM). Importantly, the distinction in cleavage behavior resulted from interactions with the peptoid residue and allosteric sites on the enzyme required for optimal activity. More recently, Groborz *et al.* also demonstrated that by incorporating unnatural amino acids into the cleavage site, they could design FRET substrates with enhanced specificity towards distinct members of the neutrophil serine proteases.¹⁹⁸ Specifically, they designed three libraries with unnatural amino acids and screened them against Cathepsin G in order to identify the most optimal substrate. The screening results allowed them to conclude that by changing one amino acid residue in the peptide backbone, they could obtain specificity towards Cathepsin G over other closely related members within the serine protease family. They validated substrate specificity *in vitro* against human neutrophil elastase.

5.3 Dictating Dynamic Hierarchical Responses

Substantial progress has been made in peptide based self-assembled materials for dynamic detection, although limitations remain. Developing design rules to control supramolecular organization and morphology while maintaining desired sensing function requires a thorough investigation of the material properties dictating hierarchical organization such as size, shape and charge. Employing

these strategies, Son *et al.* presented a modular platform to customize surface charge, supramolecular organization and enzyme specificity of peptide nanostructure with the exchange of just a few, simple amino acids.²⁰² By using the rational design of self-assembling peptide amphiphiles, they demonstrate the ability to control enzyme engagement and susceptibility to dictate final material structure (disassembly, morphology switch, etc.), successfully producing 12 unique nanostructures upon MMP-9 exposure. Using this systematic customization approach, they demonstrate the ability to predetermine material response kinetics for potential use in a variety of biomedical applications—from the selective killing of cancer cells to the delivery of drugs and imaging agents.

Despite progress towards customizing morphology and response kinetics of peptide nanostructures through systematic design, traditional self-assembling peptide amphiphiles are still limited by their proteolytic instability towards off-target species. The use of non-natural structures, such as peptoids or β -peptides, can again address these limitations, while also offering distinct advantages in the area of self-assembled materials.²⁵² In particular, their sequence-definition, ease of synthesis, and versatile side-chain chemistry allow for a broad range of functionality in application. For example, Luo *et al.* recently demonstrated a new class of dynamic nanotubes by assembling sequence-defined peptoids in a unique “rolling-up” process.²⁵³ By co-assembling ligand-tagged tube-forming peptoids, they created a multifunctional system for targeted tumor imaging and chemo-photodynamic therapy. Notably, their system was able to track intracellular generation of $^1\text{O}_2$ and correlate it to enhanced activities of caspase 3/7. In summary, the sequence-definition, bio-orthogonality, and chemical diversity of peptidomimetics may create a promising new class of sensors with a range of functionality in application.²⁵⁴

Section 6: Conclusion/Outlook

Biomaterials chemistry has provided a substantial toolbox for engineering sensing elements and transducing components amenable to detection *in vivo*. Numerous contributions have resulted in a strong repertoire of stimuli-responsive macromolecular materials able to target specific enzymatic and oxidative responses, but their interplay remains an obstacle for accurate sensing applicable in inflammatory disease diagnosis. Our hope is that this review enacts a perspective shift in material design wherein the global environment of application is considered in the fundamental conception of new ideas. We feel this evaluation merits further characterization of existing chemistries to better understand their response to multiplexed stimuli and aims to encourage continued creativity able to advance the field’s ability to meet the “ideal” biosensing criteria outlined in this review: dynamic, sensitive, specific, and selective. Considered together, we believe this toolbox of stimuli-sensitive macromolecular materials will provide strategies to incorporate multiple domains for different sensing elements, as well as the ability to form ordered structures for signal amplification. We anticipate the continued development of bioinspired synthetic

techniques will find valuable application in realizing design rules which dictate the balance between stability and susceptibility in cellular environments. Recalling the original landscape outlined in Figure 1, we envision comprehensive characterization of systems to determine where they lie on the spectra of enzymatic and oxidative susceptibility and what design components can be incorporated to shift those responses for tailored application.

Conflicts of interest

There are no conflicts to declare.

Acknowledgements

This work was supported by a Career Award at the Scientific Interfaces (#1015895) from the Burroughs Wellcome Fund (to A.M.R) and the National Institute of Health (NIH EB015007, to L.J.S.). Additional research support was provided by the National Science Foundation through the Center for Dynamics and Control of Materials: an NSF Materials Research Science and Engineering Center under Cooperative Agreement DMR-1720595.

Notes and references

- 1 Y. Lu, A. A. Aimetti, R. Langer and Z. Gu, *Nat. Rev. Mater.*, DOI:10.1038/natrevmats.2016.75.
- 2 B. A. Badeau and C. A. DeForest, *Annu. Rev. Biomed. Eng.*, 2019, **21**, 241–265.
- 3 H. R. Culver, J. R. Clegg and N. A. Peppas, *Acc. Chem. Res.*, 2017, **50**, 170–178.
- 4 C. López-Otín and J. S. Bond, *J. Biol. Chem.*, 2008, **283**, 30433–30437.
- 5 T. Gupta, Prachi; Lakes, Andrew; Dziubla, in *Oxidative Stress and Biomaterials*, Elsevier, 2016, pp. 1–33.
- 6 E. Hutter and D. Maysinger, *Trends Pharmacol. Sci.*, 2013, **34**, 497–507.
- 7 A. B. Asha, S. Srinivas, X. Hao and R. Narain, in *Smart Polymers and their Applications*, Elsevier, 2019, pp. 155–189.
- 8 G. Saravanakumar, J. Kim and W. J. Kim, *Adv. Sci.*, 2017, **4**, 1600124.
- 9 J. B. Lee, Y. M. Shin, W. S. Kim, S. Y. Kim and H.-J. Sung, in *Biomimetic Medical Materials: From Nanotechnology to 3D Bioprinting*, ed. I. Noh, Springer Singapore, Singapore, 2018, pp. 237–251.
- 10 H. Ye, Y. Zhou, X. Liu, Y. Chen, S. Duan, R. Zhu, Y. Liu and L. Yin, *Biomacromolecules*, 2019, **20**, 2441–2463.
- 11 S. Joshi-Barr, C. De Gracia Lux, E. Mahmoud and A. Almutairi, *Antioxidants Redox Signal.*, 2014, **21**, 730–754.
- 12 S. Chatterjee, in *Oxidative Stress and Biomaterials*, Elsevier, 2016, pp. 35–58.
- 13 S. H. Lee, M. K. Gupta, J. B. Bang, H. Bae and H. J. Sung, *Adv. Healthc. Mater.*, 2013, **2**, 908–915.
- 14 K.-C. Yan, A. C. Sedgwick, Y. Zang, G.-R. Chen, X.-P. He, J. Li, J. Yoon and T. D. James, *Small Methods*, 2019, 1900013.
- 15 Q. Xu, C. He, C. Xiao and X. Chen, *Macromol. Biosci.*, 2016, **16**, 635–646.
- 16 A. Stubelius, S. Lee and A. Almutairi, *Acc. Chem. Res.*, 2019, **52**, 3108–3119.
- 17 B. Adjei, Isaac M; Plumton, Glendon; Sharma, in *Oxidative Stress and Biomaterials*, Elsevier, 2016, pp. 89–115.
- 18 J. Hu, G. Zhang and S. Liu, *Chem. Soc. Rev.*, 2012, **41**, 5933–5949.
- 19 A. Napoli, M. Valentini, N. Tirelli, M. Müller and J. A. Hubbell, *Nat. Mater.*, 2004, **3**, 183–189.
- 20 C. Yang, Q. Wang and W. Ding, *RSC Adv.*, 2019, **9**, 25285–25302.
- 21 Q. Hu, P. S. Katti and Z. Gu, *Nanoscale*, 2014, **6**, 12273–12286.
- 22 M. Funovics, R. Weissleder and C. H. Tung, *Anal. Bioanal. Chem.*, 2003, **377**, 956–963.
- 23 M. Zelzer, S. J. Todd, A. R. Hirst, T. O. McDonald and R. V Ulijn, *Biomater. Sci.*, 2013, **1**, 11–39.
- 24 J. Mu, J. Lin, P. Huang and X. Chen, *Chem. Soc. Rev.*, 2018, **47**, 5554–5573.
- 25 Y. Ou, R. E. Wilson and S. G. Weber, *Annu. Rev. Anal. Chem.*, 2018, **11**, 509–533.
- 26 J. F. Woolley, J. Stanicka and T. G. Cotter, *Trends Biochem. Sci.*, 2013, **38**, 556–565.
- 27 K. Welsler, R. Adsley, B. M. Moore, W. C. Chan and J. W. Aylott, *Analyst*, 2011, **136**, 29–41.
- 28 J. R. Martin and C. L. Duvall, in *Oxidative Stress and Biomaterials*, Elsevier, 2016, pp. 225–250.
- 29 J. Sies, Helmut; Berndt, Carsten; Dean, *Annu. Rev. Biochem.*, 2017, **86**, 485–514.
- 30 C. Nathan and A. Cunningham-Bussell, *Nat. Rev. Immunol.*, 2013, **13**, 349–361.
- 31 C. T. N. Pham, *Nat. Rev. Immunol.*, 2006, **6**, 541–550.
- 32 J. Lugrin, N. Rosenblatt-Velin, R. Parapanov and L. Liaudet, *Biol. Chem.*, 2014, **395**, 203–230.
- 33 J. Frijhoff, P. G. Winyard, N. Zarkovic, S. S. Davies, R. Stocker, D. Cheng, A. R. Knight, E. L. Taylor, J. Oettrich, T. Ruskovska, A. C. Gasparovic, A. Cuadrado, D. Weber, H. E. Poulsen, T. Grune, H. H. W. Schmidt and P. Ghezzi, *Antioxidants Redox Signal.*, 2015, **23**, 1144–1170.
- 34 J. Wang, H. Zhang, F. Wang, X. Ai, D. Huang, G. Liu and P. Mi, in *Stimuli Responsive Polymeric Nanocarriers for Drug Delivery Applications, Volume 1*, Elsevier, 2018, pp. 101–119.
- 35 R. Roy, J. Yang and M. A. Moses, *J. Clin. Oncol.*, 2009, **27**, 5287–5297.
- 36 R. Ramachandran, C. Altier, K. Oikonomopoulou and M. D. Hollenberg, *Pharmacol. Rev.*, 2016, **68**, 1110–1142.
- 37 F. J. Garcia and K. S. Carroll, *Eur. J. Med. Chem.*, 2014, **88**, 28–33.
- 38 R. Karisch and B. G. Neel, *FEBS J.*, 2013, **280**, 459–475.
- 39 B. L. Zervas and D. J. Trader, *J. Am. Chem. Soc.*, 2019, **141**, 5252–5260.
- 40 N. M. Mishina, I. Bogeski, D. A. Bolotin, M. Hoth, B. A. Niemeyer, C. Schultz, E. V. Zagaynova, S. Lukyanov and V. V. Belousov, *Antioxidants Redox Signal.*, 2012, **17**, 505–512.
- 41 V. J. Thannickal and B. L. Fanburg, *Am. J. Physiol. - Lung Cell. Mol. Physiol.*, DOI:10.1152/ajplung.2000.279.6.11005.
- 42 C. L. Hsieh, C. M. Liu, H. A. Chen, S. T. Yang, K. Shigemura, K. Kitagawa, F. Yamamichi, M. Fujisawa, Y. R. Liu, W. H. Lee, K. C. Chen, C. N. Shen, C. C. Lin, L. W. K. Chung and S. Y. Sung, *Sci. Rep.*, DOI:10.1038/s41598-017-08835-9.
- 43 K. Mori, T. Uchida, T. Yoshie, Y. Mizote, F. Ishikawa, M. Katsuyama and M. Shibamura, *FEBS J.*, 2019, **286**, 459–

- 478.
- 44 W. J. Peveler, M. Yazdani and V. M. Rotello, *ACS Sensors*, 2016, **1**, 1282–1285.
- 45 U. Haedke, E. V. Küttler, O. Vosyka, Y. Yang and S. H. L. Verhelst, *Curr. Opin. Chem. Biol.*, 2013, **17**, 102–109.
- 46 D. R. Brenner, D. Scherer, K. Muir, J. Schildkraut, P. Boffetta, M. R. Spitz, L. Le Marchand, A. T. Chan, E. L. Goode, C. M. Ulrich and R. J. Hung, *Cancer Epidemiol. Biomarkers Prev.*, 2014, **23**, 1729–1751.
- 47 M. Holzinger, A. Le Goff and S. Cosnier, *Front. Chem.*, DOI:10.3389/fchem.2014.00063.
- 48 P. D. Howes, R. Chandrawati and M. M. Stevens, *Science (80-.)*, 2014, **346**, 1247390.
- 49 A. Othman, A. Karimi and S. Andreescu, *J. Mater. Chem. B*, 2016, **4**, 7178–7203.
- 50 P. Mehrotra, *J. Oral Biol. Craniofacial Res.*, 2016, **6**, 153–159.
- 51 M. A. Cooper, *Nat. Rev. Drug Discov.*, 2002, **1**, 515–528.
- 52 Y. Jiang, M. Wang, J. Hardie, G. Y. Tonga, M. Ray, Q. Xu and V. M. Rotello, *Small*, 2016, **12**, 3775–3779.
- 53 C. De Gracia Lux, S. Joshi-Barr, T. Nguyen, E. Mahmoud, E. Schopf, N. Fomina and A. Almutairi, *J. Am. Chem. Soc.*, 2012, **134**, 15758–15764.
- 54 W. Lv, J. Xu, X. Wang, X. Li, Q. Xu and H. Xin, *ACS Nano*, 2018, **12**, 5417–5426.
- 55 R. Weinstain, E. N. Savariar, C. N. Felsen and R. Y. Tsien, *J. Am. Chem. Soc.*, 2014, **136**, 874–877.
- 56 M. L. Viger, G. Collet, J. Lux, V. A. Nguyen Huu, M. Guma, A. Foucault-Collet, J. Olejniczak, S. Joshi-Barr, G. S. Firestein and A. Almutairi, *Biomaterials*, 2017, **133**, 119–131.
- 57 Y. H. Fu, C. Y. Chen and C. T. Chen, *Polym. Chem.*, 2015, **6**, 8132–8143.
- 58 K. E. Broaders, S. Grandhe and J. M. J. Fréchet, *J. Am. Chem. Soc.*, 2011, **133**, 756–758.
- 59 V. G. Deepagan, E. K. Pramod Kumar, Y. D. Suh and J. H. Park, *Macromol. Res.*, 2018, **26**, 577–580.
- 60 H. Ren, Y. Wu, N. Ma, H. Xu and X. Zhang, *Soft Matter*, 2012, **8**, 1460–1466.
- 61 P. Han, N. Ma, H. Ren, H. Xu, Z. Li, Z. Wang and X. Zhang, *Langmuir*, 2010, **26**, 14414–14418.
- 62 N. Ma, Y. Li, H. Xu, Z. Wang and X. Zhang, *J. Am. Chem. Soc.*, 2010, **132**, 442–443.
- 63 L. Yu, Y. Yang, F. S. Du and Z. C. Li, *Biomacromolecules*, 2018, **19**, 2182–2193.
- 64 E. C. Wu, J. H. Park, J. Park, E. Segal, F. Cunin and M. J. Sailor, *ACS Nano*, 2008, **2**, 2401–2409.
- 65 S. S. Yu, R. L. Koblin, A. L. Zachman, D. S. Perrien, L. H. Hofmeister, T. D. Giorgio and H. J. Sung, *Biomacromolecules*, 2011, **12**, 4357–4366.
- 66 S. H. Lee, T. C. Boire, J. B. Lee, M. K. Gupta, A. L. Zachman, R. Rath and H. J. Sung, *J. Mater. Chem. B*, 2014, **2**, 7109–7113.
- 67 J. Ulbricht, R. Jordan and R. Luxenhofer, *Biomaterials*, 2014, **35**, 4848–4861.
- 68 K. S. Dhada, D. S. Hernandez and L. J. Suggs, *ACS Nano*, 2019, **13**, 7791–7799.
- 69 S. K. Lee, L. J. Mortensen, C. P. Lin and C. H. Tung, *Nat. Commun.*, 2014, **5**, 1–8.
- 70 F. Muhammad, W. Qi, A. Wang, J. Gu, J. Du and G. Zhu, *J. Mater. Chem. B*, 2015, **3**, 1597–1604.
- 71 C. Yin, X. Zhen, Q. Fan, W. Huang and K. Pu, *ACS Nano*, 2017, **11**, 4174–4182.
- 72 M. K. Gupta, T. A. Meyer, C. E. Nelson and C. L. Duvall, *J. Control. Release*, 2012, **162**, 591–598.
- 73 F. Muhammad, A. Wang, L. Miao, P. Wang, Q. Li, J. Liu, J. Du and G. Zhu, *Langmuir*, 2015, **31**, 514–521.
- 74 F. Muhammad, W. Qi, A. Wang, J. Gu and G. Zhu, *J. Mater. Chem. B*, 2015, **3**, 5711–5719.
- 75 Y. Shen, L. Liang, J. Zhang, Z. Li, J. Yue, J. Wang, W. Xu, W. Shi and S. Xu, *Sensors Actuators, B Chem.*, 2019, **285**, 84–91.
- 76 E. A. Mahmoud, J. Sankaranarayanan, J. M. Morachis, G. Kim and A. Almutairi, *Bioconjug. Chem.*, 2011, **22**, 1416–1421.
- 77 J. S. Kim, S. D. Jo, G. L. Seah, I. Kim and Y. S. Nam, *J. Ind. Eng. Chem.*, 2015, **21**, 1137–1142.
- 78 C. Yue, C. Zhang, G. Alfranca, Y. Yang, X. Jiang, Y. Yang, F. Pan, J. M. de la Fuente and D. Cui, *Theranostics*, 2016, **6**, 456–469.
- 79 Y. Shim, Min Suk; Xia, *Angew. Chem. Int. Ed.*, 2013, **52**, 6926–6929.
- 80 K. Han, J. Y. Zhu, S. B. Wang, Z. H. Li, S. X. Cheng and X. Z. Zhang, *J. Mater. Chem. B*, 2015, **3**, 8065–8069.
- 81 C. Sun, Y. Liang, N. Hao, L. Xu, F. Cheng, T. Su, J. Cao, W. Gao, Y. Pu and B. He, *Org. Biomol. Chem.*, 2017, **15**, 9176–9185.
- 82 S. Shi, L. Zhang, M. Zhu, G. Wan, C. Li, J. Zhang, Y. Wang and Y. Wang, *ACS Appl. Mater. Interfaces*, 2018, **10**, 29260–29272.
- 83 L. Xu, Y. Yang, M. Zhao, W. Gao, H. Zhang, S. Li, B. He and Y. Pu, *J. Mater. Chem. B*, 2018, **6**, 1076–1084.
- 84 Z. Chen, Z. Liu, Z. Li, E. Ju, N. Gao, L. Zhou, J. Ren and X. Qu, *Biomaterials*, 2015, **39**, 15–22.
- 85 Z. Huang, Q. Yao, J. Chen and Y. Gao, *Chem. Commun.*, 2018, **54**, 5385–5388.
- 86 F. Wang, X. Liu, C. H. Lu and I. Willner, *ACS Nano*, 2013, **7**, 7278–7286.
- 87 L. L. Wang, J. Qiao, L. Qi, X. Z. Xu and D. Li, *Sci. China Chem.*, 2015, **58**, 1508–1514.
- 88 W. Gao, X. Wei, X. Wang, G. Cui, Z. Liu and B. Tang, *Chem. Commun.*, 2016, **52**, 3643–3646.
- 89 Y. G. Ermakova, D. S. Bilan, M. E. Matlashov, N. M. Mishina, K. N. Markvicheva, O. M. Subach, F. V. Subach, I. Bogeski, M. Hoth, G. Enikolopov and V. V. Belousov, *Nat. Commun.*, 2014, **5**, 1–9.
- 90 B. Morgan, K. Van Laer, T. N. E. Owusu, D. Ezeriņa, D. Pastor-Flores, P. S. Amponsah, A. Tursch and T. P. Dick, *Nat. Chem. Biol.*, 2016, **12**, 437–443.
- 91 D. S. Bilan and V. V. Belousov, *Free Radic. Biol. Med.*, 2017, **109**, 167–188.
- 92 D. S. Bilan and V. V. Belousov, *Antioxidants Redox Signal.*, 2018, **29**, 569–584.
- 93 B. L. Allen, J. D. Johnson and J. P. Walker, *ACS Nano*, 2011, **5**, 5263–5272.
- 94 Z. Y. Qiao, W. J. Zhao, Y. Cong, D. Zhang, Z. Hu, Z. Y. Duan and H. Wang, *Biomacromolecules*, 2016, **17**, 1643–1652.
- 95 X. Fu, Y. Ma, Y. Shen, W. Fu and Z. Li, *Biomacromolecules*, 2014, **15**, 1055–1061.
- 96 Y. T. Chiang, Y. W. Yen and C. L. Lo, *Biomaterials*, 2015, **61**, 150–161.
- 97 J. Chang, H. Li, T. Hou, W. Duan and F. Li, *Biosens. Bioelectron.*, 2018, **104**, 152–157.
- 98 J. Liu, Y. Pang, Z. Zhu, D. Wang, C. Li, W. Huang, X. Zhu and D. Yan, *Biomacromolecules*, 2013, **14**, 1627–1636.

- 99 W. Cao, Y. Gu, T. Li and H. Xu, *Chem. Commun.*, 2015, **51**, 7069–7071.
- 100 R. H. Staff, M. Gallei, M. Mazurowski, M. Rehahn, R. Berger, K. Landfester and D. Crespy, *ACS Nano*, 2012, **6**, 9042–9049.
- 101 L. Liu, L. Rui, Y. Gao and W. Zhang, *Polym. Chem.*, 2015, **6**, 1817–1829.
- 102 R. Fang, H. Xu, W. Cao, L. Yang and X. Zhang, *Polym. Chem.*, 2015, **6**, 2817–2821.
- 103 G. Wu, F. Zeng, C. Yu, S. Wu and W. Li, *J. Mater. Chem. B*, 2014, **2**, 8528–8537.
- 104 W.-K. Oh, Y. Seon Jeong, S. Kim and J. Jang, , DOI:10.1021/nn204899m.
- 105 F. Du, Y. Min, F. Zeng, C. Yu and S. Wu, *Small*, 2014, **10**, 964–972.
- 106 M. Zhuang, C. Ding, A. Zhu and Y. Tian, *Anal. Chem.*, 2014, **86**, 1829–1836.
- 107 J. Qiao, Z. Liu, Y. Tian, M. Wu and Z. Niu, *Chem. Commun.*, 2015, **51**, 3641–3644.
- 108 Z. Song, D. Mao, S. H. P. Sung, R. T. K. Kwok, J. W. Y. Lam, D. Kong, D. Ding and B. Z. Tang, *Adv. Mater.*, 2016, **28**, 7249–7256.
- 109 G. Li, D. Zhu, Q. Liu, L. Xue and H. Jiang, *Org. Lett.*, 2013, **15**, 924–927.
- 110 K. Zhou, F. Zhang, J. Xu, H. He, W. Wei, Z. Xia, K. Zhou, F. Zhang, J. Xu, H. He, W. Wei and Z. Xia, *Part. Part. Syst. Charact.*, , DOI:10.1002/ppsc.201700329.
- 111 Y. D. Lee, C. K. Lim, A. Singh, J. Koh, J. Kim, I. C. Kwon and S. Kim, *ACS Nano*, 2012, **6**, 6759–6766.
- 112 D. Lee, S. Khaja, J. C. Velasquez-Castano, M. Dasari, C. Sun, J. Petros, W. R. Taylor and N. Murthy, *Nat. Mater.*, 2007, **6**, 765–769.
- 113 Y. Cui, F. Chen and X. B. Yin, *Biosens. Bioelectron.*, 2019, **135**, 208–215.
- 114 M. Sk, S. Banesh, V. Trivedi and S. Biswas, *Inorg. Chem.*, 2018, **57**, 14574–14581.
- 115 Y. H. Seo, A. Singh, H. J. Cho, Y. Kim, J. Heo, C. K. Lim, S. Y. Park, W. D. Jang and S. Kim, *Biomaterials*, 2016, **84**, 111–118.
- 116 C. Y. Chen and C. T. Chen, *Chem. - A Eur. J.*, 2013, **19**, 16050–16057.
- 117 A. Singh, Y. H. Seo, C. K. Lim, J. Koh, W. D. Jang, I. C. Kwon and S. Kim, *ACS Nano*, 2015, **9**, 9906–9911.
- 118 J. Liu, Z. Z. Dong, C. Yang, G. Li, C. Wu, F. W. Lee, C. H. Leung and D. L. Ma, *Sci. Rep.*, , DOI:10.1038/s41598-017-09478-6.
- 119 X. Cao, S. Cheng, Y. You, S. Zhang and Y. Xian, *Anal. Chim. Acta*, , DOI:10.1016/j.aca.2019.09.051.
- 120 X. Hu, X. Liu, X. Zhang, H. Chai and Y. Huang, *Biosens. Bioelectron.*, 2018, **105**, 65–70.
- 121 Q. Zhao, R. Zhang, D. Ye, S. Zhang, H. Chen and J. Kong, *ACS Appl. Mater. Interfaces*, 2017, **9**, 2052–2058.
- 122 C. C. Winterbourn, *Nat. Chem. Biol.*, 2008, **4**, 278–286.
- 123 M. B. Grisham, *Comp. Biochem. Physiol. - A Mol. Integr. Physiol.*, 2013, **165**, 429–438.
- 124 P. Wardman, *Free Radic. Biol. Med.*, 2007, **43**, 995–1022.
- 125 C. C. Winterbourn, *Biochim. Biophys. Acta - Gen. Subj.*, 2014, **1840**, 730–738.
- 126 X. Huang, T. Lan, B. Zhang and J. Ren, *Analyst*, 2012, **137**, 3659–3666.
- 127 B. S. Berlett and E. R. Stadtman, *J. Biol. Chem.*, 1997, **272**, 20313–20316.
- 128 R. Torosantucci, C. Schöneich and W. Jiskoot, *Pharm. Res.*, 2014, **31**, 541–553.
- 129 B. Ezraty, A. Gennaris, F. Barras and J. F. Collet, *Nat. Rev. Microbiol.*, 2017, **15**, 385–396.
- 130 E. R. Stadtman and R. L. Levine, *Amino Acids*, 2003, **25**, 207–218.
- 131 A. Amici, R. L. Levine, L. Tsai and E. R. Stadtman, *J. Biol. Chem.*, 1989, **264**, 3341–3346.
- 132 H. Guo, H. Aleyasin, B. C. Dickinson, R. E. Haskew-Layton and R. R. Ratan, *Cell Biosci.*, , DOI:10.1186/2045-3701-4-64.
- 133 A. Baruch, D. A. Jeffery and M. Bogyo, *Trends Cell Biol.*, 2004, **14**, 29–35.
- 134 L. Yuan, W. Lin, K. Zheng and S. Zhu, *Acc. Chem. Res.*, 2013, **46**, 1462–1473.
- 135 J. Shi, F. Tian, J. Lyu and M. Yang, *J. Mater. Chem. B*, 2015, **3**, 6989–7005.
- 136 S. M. Ng, M. Koneswaran and R. Narayanaswamy, *RSC Adv.*, 2016, **6**, 21624–21661.
- 137 H. Dong, W. Gao, F. Yan, H. Ji and H. Ju, *Anal. Chem.*, 2010, **82**, 5511–5517.
- 138 A. M. Smith and S. Nie, *Acc. Chem. Res.*, 2010, **43**, 190–200.
- 139 X. Cao, S. Cheng, Y. You, S. Zhang and Y. Xian, *Anal. Chim. Acta*, , DOI:10.1016/j.aca.2019.09.051.
- 140 R. Weissleder, *Nat. Biotechnol.*, 2001, **19**, 316–317.
- 141 K. Saha, S. S. Agasti, C. Kim, X. Li and V. M. Rotello, *Chem. Rev.*, 2012, **112**, 2739–2779.
- 142 C. C. You, O. R. Miranda, B. Gider, P. S. Ghosh, I. B. Kim, B. Erdogan, S. A. Krovi, U. H. F. Bunz and V. M. Rotello, *Nat. Nanotechnol.*, 2007, **2**, 318–323.
- 143 J. I. Cutler, E. Auyeung and C. A. Mirkin, *J. Am. Chem. Soc.*, 2012, **134**, 1376–1391.
- 144 I. Willner and B. Willner, *Nano Lett.*, 2010, **10**, 3805–3815.
- 145 Y. Kurishita, T. Kohira, A. Ojida and I. Hamachi, *J. Am. Chem. Soc.*, 2010, **132**, 13290–13299.
- 146 M. Schäferling and A. Duerkop, in *Standardization and Quality Assurance in Fluorescence Measurements I: Techniques*, ed. U. Resch-Genger, Springer Berlin Heidelberg, Berlin, Heidelberg, 2008, pp. 373–414.
- 147 C. Moore, F. Chen, J. Wang and J. V. Jokerst, *Adv. Drug Deliv. Rev.*, 2019, **144**, 78–89.
- 148 Q. Miao and K. Pu, *Bioconjug. Chem.*, 2016, **27**, 2808–2823.
- 149 J. Weber, P. C. Beard and S. E. Bohndiek, *Nat. Methods*, 2016, **13**, 639–650.
- 150 Q. Zhang, F. Zhang, Y. Chen, Y. Dou, H. Tao, D. Zhang, R. Wang, X. Li and J. Zhang, *Chem. Mater.*, 2017, **29**, 8221–8238.
- 151 S. Erbas-Cakmak, S. Kolemen, A. C. Sedgwick, T. Gunnlaugsson, T. D. James, J. Yoon and E. U. Akkaya, *Chem. Soc. Rev.*, 2018, **47**, 2228–2248.
- 152 A. C. Sedgwick, H. H. Han, J. E. Gardiner, S. D. Bull, X. P. He and T. D. James, *Chem. Sci.*, 2018, **9**, 3672–3676.
- 153 L. B. Poole, *Free Radic. Biol. Med.*, 2015, **80**, 148–157.
- 154 E. C. Greenwald, S. Mehta and J. Zhang, *Chem. Rev.*, 2018, **118**, 11707–11794.
- 155 D. S. Bilan, L. Pase, L. Joosen, A. Y. Gorokhovatsky, Y. G. Ermakova, T. W. J. Gadella, C. Grabher, C. Schultz, S. Lukyanov and V. V. Belousov, *ACS Chem. Biol.*, 2013, **8**, 535–542.
- 156 K. N. Markvicheva, D. S. Bilan, N. M. Mishina, A. Y. Gorokhovatsky, L. M. Vinokurov, S. Lukyanov and V. V. Belousov, *Bioorganic Med. Chem.*, 2011, **19**, 1079–1084.
- 157 R. Tao, Y. Zhao, H. Chu, A. Wang, J. Zhu, X. Chen, Y. Zou, M.

- Shi, R. Liu, N. Su, J. Du, H. M. Zhou, L. Zhu, X. Qian, H. Liu, J. Loscalzo and Y. Yang, *Nat. Methods*, 2017, **14**, 720–728.
- 158 P. Kasperkiewicz, M. Poreba, K. Groborz and M. Drag, *FEBS J.*, 2017, **284**, 1518–1539.
- 159 F. Li, Y. Wang, C. Li, T. T. Marquez-Lago, A. Leier, N. D. Rawlings, G. Haffari, J. Revote, T. Akutsu, K.-C. Chou, A. W. Purcell, R. N. Pike, G. I. Webb, A. Ian Smith, T. Lithgow, R. J. Daly, J. C. Whisstock and J. Song, *Brief. Bioinform.*, 2018, **00**, 1–17.
- 160 M. Schaeperl, J. E. Fuchs, B. J. Waldner, R. G. Huber, C. Kramer and K. R. Liedl, *PLoS One*, 2015, **10**, 1–17.
- 161 X. Wang, M. Gu, T. B. Toh, N. L. B. Abdullah and E. K. H. Chow, *SLAS Technol.*, 2018, **23**, 44–56.
- 162 S. Lee, E. J. Cha, K. Park, S. Y. Lee, J. K. Hong, I. C. Sun, S. Y. Kim, K. Choi, I. C. Kwon, K. Kim and C. H. Ahn, *Angew. Chemie - Int. Ed.*, 2008, **47**, 2804–2807.
- 163 Y. P. Kim, W. L. Daniel, Z. Xia, H. Xie, C. A. Mirkin and J. Rao, *Chem. Commun.*, 2010, **46**, 76–78.
- 164 I. C. Sun, S. Lee, H. Koo, I. C. Kwon, K. Choi, C. H. Ahn and K. Kim, *Bioconjug. Chem.*, 2010, **21**, 1939–1942.
- 165 S. Y. Park, S. M. Lee, G. B. Kim and Y. P. Kim, *Gold Bull.*, 2012, **45**, 213–219.
- 166 C. J. Mu, D. A. LaVan, R. S. Langer and B. R. Zetter, *ACS Nano*, 2010, **4**, 1511–1520.
- 167 Y. Wang, P. Shen, C. Li, Y. Wang and Z. Liu, *Anal. Chem.*, 2012, **84**, 1466–1473.
- 168 Y. Shi, C. Yi, Z. Zhang, H. Zhang, M. Li, M. Yang and Q. Jiang, *ACS Appl. Mater. Interfaces*, 2013, **5**, 6494–6501.
- 169 F. Chen, G. Hableel, E. R. Zhao and J. V. Jokerst, *J. Colloid Interface Sci.*, 2018, **521**, 261–279.
- 170 P. D. Nguyen, V. T. Cong, C. Baek and J. Min, *Biosens. Bioelectron.*, 2017, **89**, 666–672.
- 171 X. Xia, M. Yang, L. K. Oetjen, Y. Zhang, Q. Li, J. Chen and Y. Xia, *Nanoscale*, 2011, **3**, 950–953.
- 172 K. Boeneman, B. C. Mei, A. M. Dennis, G. Bao, J. R. Deschamps, H. Mattoussi and I. L. Medintz, *J. Am. Chem. Soc.*, 2009, **131**, 3828–3829.
- 173 S. B. Lowe, J. A. G. Dick, B. E. Cohen and M. M. Stevens, *ACS Nano*, 2012, **6**, 851–857.
- 174 R. Freeman, T. Finder, R. Gill and I. Willner, *Nano Lett.*, 2010, **10**, 2192–2196.
- 175 H. Yao, Y. Zhang, F. Xiao, Z. Xia and J. Rao, *Angew. Chemie - Int. Ed.*, 2007, **46**, 4346–4349.
- 176 Z. Wang, X. Li, Y. Song, L. Li, W. Shi and H. Ma, *Anal. Chem.*, 2015, **87**, 5816–5823.
- 177 J. Liu, L. Zhang, J. Lei, H. Shen and H. Ju, *ACS Appl. Mater. Interfaces*, 2017, **9**, 2150–2158.
- 178 H. Shen, J. Liu, J. Lei and H. Ju, *Chem. Commun.*, 2018, **54**, 9155–9158.
- 179 W. Yang, G. Zhang, W. Weng, B. Qiu, L. Guo, Z. Lin and G. Chen, *RSC Adv.*, 2014, **4**, 58852–58857.
- 180 X. Yin, B. Yang, B. Chen, M. He and B. Hu, *Anal. Chem.*, 2019, **91**, 10596–10603.
- 181 S. L. Sewell and T. D. Giorgio, *Mater. Sci. Eng. C*, 2009, **29**, 1428–1432.
- 182 A. Lee, S. H. Kim, H. Lee, B. Kim, Y. S. Kim and J. Key, *Nanomaterials*, DOI:10.3390/nano8020119.
- 183 I. L. Medintz, A. R. Clapp, F. M. Brunel, T. Tiefenbrunn, H. Tetsuo Uyeda, E. L. Chang, J. R. Deschamps, P. E. Dawson and H. Mattoussi, *Nat. Mater.*, 2006, **5**, 581–589.
- 184 A. J. De Graaf, E. Mastrobattista, T. Vermonden, C. F. Van Nostrum, D. T. S. Rijkers, R. M. J. Liskamp and W. E. Hennink, *Macromolecules*, 2012, **45**, 842–851.
- 185 L. Yin, H. Sun, H. Zhang, L. He, L. Qiu, J. Lin, H. Xia, Y. Zhang, S. Ji, H. Shi and M. Gao, *J. Am. Chem. Soc.*, 2019, **141**, 3265–3273.
- 186 K. Park, J. Jeong and B. H. Chung, *Chem. Commun.*, 2012, **48**, 10547–10549.
- 187 X. Gao, J. Li, M. Luan, Y. Li, W. Pan, N. Li and B. Tang, *Biosens. Bioelectron.*, DOI:10.1016/j.bios.2019.111755.
- 188 K. Q. Luo, V. C. Yu, Y. Pu and D. C. Chang, *Biochem. Biophys. Res. Commun.*, 2001, **283**, 1054–1060.
- 189 F. A. Jaffer, D. E. Kim, L. Quinti, C. H. Tung, E. Aikawa, A. N. Pande, R. H. Kohler, G. P. Shi, P. Libby and R. Weissleder, *Circulation*, 2007, **115**, 2292–2298.
- 190 Y. Ni, Z. Hai, T. Zhang, Y. Wang, Y. Yang, S. Zhang and G. Liang, *Anal. Chem.*, 2019, **91**, 14834–14837.
- 191 D. Kim, Y. Lee, S. Jo, S. Kim and T. Seung, *Sensors Actuators B. Chem.*, 2020, **307**, 127641.
- 192 J. Andrieu, N. Kotman, M. Maier, V. Mailänder, W. S. L. Strauss, C. K. Weiss and K. Landfester, *Macromol. Rapid Commun.*, 2012, **33**, 248–253.
- 193 R. Heim and R. Y. Tsien, *Curr. Biol.*, 1996, **6**, 178–182.
- 194 W. J. Akers, B. Xu, H. Lee, G. P. Sudlow, G. B. Fields, S. Achilefu and W. B. Edwards, *Bioconjug. Chem.*, 2012, **23**, 656–663.
- 195 M. Stawarski, I. Rutkowska-Wlodarczyk, A. Zeug, M. Bijata, H. Madej, L. Kaczmarek and J. Wlodarczyk, *Biomaterials*, 2014, **35**, 1402–1410.
- 196 S. Talley, O. Kalinina, M. Winek, W. Paik, A. R. Cannon, F. Alonzo, M. A. Choudhry, K. L. Knight and E. M. Campbell, *J. Immunol.*, 2019, **ji1900619**.
- 197 M. J. Stawikowski, R. Stawikowska and G. B. Fields, *Biochemistry*, 2015, **54**, 3110–3121.
- 198 K. Groborz, S. Kott, P. Kasperkiewicz and M. Drag, *Biochimie*, 2019, **166**, 103–111.
- 199 S. K. Lee, M. S. Han and C. H. Tung, *Small*, 2012, **8**, 3315–3320.
- 200 K. Yang, M. Liu, Y. Wang, S. Wang, H. Miao, L. Yang and X. Yang, *Sensors Actuators, B Chem.*, 2017, **251**, 503–508.
- 201 D. Koda, T. Maruyama, N. Minakuchi, K. Nakashima and M. Goto, *Chem. Commun.*, 2010, **46**, 979–981.
- 202 J. Son, D. Kalafatovic, M. Kumar, B. Yoo, M. A. Cornejo, M. Contel and R. V. Uljin, *ACS Nano*, 2019, **13**, 1555–1562.
- 203 Y. Cheng, F. Huang, X. Min, P. Gao, T. Zhang, X. Li, B. Liu, Y. Hong, X. Lou and F. Xia, *Anal. Chem.*, 2016, **88**, 8913–8919.
- 204 T. H. Ku, M. P. Chien, M. P. Thompson, R. S. Sinkovits, N. H. Olson, T. S. Baker and N. C. Gianneschi, *J. Am. Chem. Soc.*, 2011, **133**, 8392–8395.
- 205 Y. Yuan, R. T. K. Kwok, B. Z. Tang and B. Liu, *J. Am. Chem. Soc.*, 2014, **136**, 2546–2554.
- 206 D. Ye, A. J. Shuhendler, L. Cui, L. Tong, S. S. Tee, G. Tikhomirov, D. W. Felsher and J. Rao, *Nat. Chem.*, 2014, **6**, 519–526.
- 207 Y. Xu, W. Shi, X. He, X. Wu, X. Li and H. Ma, *Anal. Chem.*, 2017, **89**, 10980–10984.
- 208 H. Koga, R. Toita, T. Mori, T. Tomiyama, J. H. Kang, T. Niidome and Y. Katayama, *Bioconjug. Chem.*, 2011, **22**, 1526–1534.
- 209 C. Wang, Q. Chen, Z. Wang and X. Zhang, *Angew. Chemie - Int. Ed.*, 2010, **49**, 8612–8615.
- 210 X. Li, Z. Zhou, Y. Tang, C. Cheng Zhang, Y. Zheng, J. Gao and Q. Wang, *Sensors Actuators, B Chem.*, 2018, **276**, 95–100.
- 211 R. Chib, M. Mummert, I. Bora, B. W. Laursen, S. Shah, R.

- Pendry, I. Gryczynski, J. Borejdo, Z. Gryczynski and R. Fudala, *Anal. Bioanal. Chem.*, 2016, **408**, 3811–3821.
- 212 H. Xie, F. Zeng and S. Wu, *Biomacromolecules*, 2014, **15**, 3383–3389.
- 213 E. Schellenberger, F. Rudloff, C. Warmuth, M. Taupitz, B. Hamm and J. Schnorr, *Bioconjug. Chem.*, 2008, **19**, 2440–2445.
- 214 Z. Sun, K. Cheng, Y. Yao, F. Wu, J. Fung, H. Chen, X. Ma, Y. Tu, L. Xing, L. Xia and Z. Cheng, *ACS Nano*, 2019, **13**, 1153–1167.
- 215 G. B. Kim, K. H. Kim, Y. H. Park, S. Ko and Y. P. Kim, *Biosens. Bioelectron.*, 2013, **41**, 833–839.
- 216 G. Von Maltzahn, T. J. Harris, J. H. Park, D. H. Min, A. J. Schmidt, M. J. Sailor and S. N. Bhatia, *J. Am. Chem. Soc.*, 2007, **129**, 6064–6065.
- 217 J. Gallo, N. Kamaly, I. Lavdas, E. Stevens, Q. De Nguyen, M. Wylezinska-Arridge, E. O. Aboagye and N. J. Long, *Angew. Chemie - Int. Ed.*, 2014, **53**, 9550–9554.
- 218 J. H. Kim and B. H. Chung, *Small*, 2010, **6**, 126–131.
- 219 Y. Pan, M. Guo, Z. Nie, Y. Huang, Y. Peng, A. Liu, M. Qing and S. Yao, *Chem. Commun.*, 2012, **48**, 997–999.
- 220 G. Von Maltzahn, D. H. Min, Y. Zhang, J. H. Park, T. J. Harris, M. Sailor and S. N. Bhatia, *Adv. Mater.*, 2007, **19**, 3579–3583.
- 221 T. Serizawa, Y. Hirai and M. Aizawa, *Mol. Biosyst.*, 2010, **6**, 1565–1568.
- 222 J. Oishi, Y. Asami, T. Mori, J. H. Kang, T. Niidome and Y. Katayama, *Biomacromolecules*, 2008, **9**, 2301–2308.
- 223 S. Gupta, H. Andresen, J. E. Ghadiali and M. M. Stevens, *Small*, 2010, **6**, 1509–1513.
- 224 H. Jiao, J. Chen, W. Li, F. Wang, H. Zhou, Y. Li and C. Yu, *ACS Appl. Mater. Interfaces*, 2014, **6**, 1979–1985.
- 225 Z. Wang, R. Lévy, D. G. Fernig and M. Brust, *J. Am. Chem. Soc.*, 2006, **128**, 2214–2215.
- 226 H. Bui, C. W. Brown, S. Buckhout-White, S. A. Díaz, M. H. Stewart, K. Susumu, E. Oh, M. G. Ancona, E. R. Goldman and I. L. Medintz, *Small*, 2019, **15**, 1–13.
- 227 H. Kitazaki, T. Mori, J. H. Kang, T. Niidome, M. Murata, M. Hashizume and Y. Katayama, *Colloids Surfaces B Biointerfaces*, 2012, **99**, 7–11.
- 228 G. Lu, S. Li, Z. Guo, O. K. Farha, B. G. Hauser, X. Qi, Y. Wang, X. Wang, S. Han, X. Liu, J. S. Duchene, H. Zhang, Q. Zhang, X. Chen, J. Ma, S. C. J. Loo, W. D. Wei, Y. Yang, J. T. Hupp and F. Huo, *Nat. Chem.*, 2012, **4**, 310–316.
- 229 A. Prinz, G. Reither, M. Diskar and C. Schultz, *Proteomics*, 2008, **8**, 1179–1196.
- 230 M. K. So, C. Xu, A. M. Loening, S. S. Gambhir and J. Rao, *Nat. Biotechnol.*, 2006, **24**, 339–343.
- 231 P. R. Selvin, *Nat. Struct. Biol.*, 2000, **7**, 730–734.
- 232 M. J. Webber, *Bioeng. Transl. Med.*, 2016, **1**, 252–266.
- 233 T. L. Mako, J. M. Racicot and M. Levine, *Chem. Rev.*, 2019, **119**, 322–477.
- 234 I. V. Kolesnichenko and E. V. Anslyn, *Chem. Soc. Rev.*, 2017, **46**, 2385–2390.
- 235 M. J. Webber, C. J. Newcomb, R. Bitton and S. I. Stupp, *Soft Matter*, 2011, **7**, 9665–9672.
- 236 R. Weissleder, M. Nahrendorf and M. J. Pittet, *Nat. Mater.*, 2014, **13**, 125–138.
- 237 E. Y. Kim, D. Kumar, G. Khang and D. K. Lim, *J. Mater. Chem. B*, 2015, **3**, 8433–8444.
- 238 D. Maysinger and E. Hutter, *Nanomedicine*, 2015, **10**, 483–501.
- 239 P. D. Howes, S. Rana and M. M. Stevens, *Chem. Soc. Rev.*, 2014, **43**, 3835–3853.
- 240 H. Heinz, C. Pramanik, O. Heinz, Y. Ding, R. K. Mishra, D. Marchon, R. J. Flatt, I. Estrela-Lopis, J. Llop, S. Moya and R. F. Ziolo, *Surf. Sci. Rep.*, 2017, **72**, 1–58.
- 241 Z. Wang, J. Lee, A. R. Cossins and M. Brust, *Anal. Chem.*, 2005, **77**, 5770–5774.
- 242 J. Li, A. A. Green, H. Yan and C. Fan, *Nat. Chem.*, 2017, **9**, 1056–1067.
- 243 Y. Shim, Min Suk; Xia, *Angew. Chem. Int. Ed.*, 2013, **52**, 6926–6929.
- 244 M. J. Austin and A. M. Rosales, *Biomater. Sci.*, 2019, **7**, 490–505.
- 245 P. Free, C. P. Shaw and R. Lévy, *Chem. Commun.*, 2009, 5009–5011.
- 246 R. Kumar, A. N. Maitra, P. K. Patanjali and P. Sharma, *Biomaterials*, 2005, **26**, 6743–6753.
- 247 A. M. Aldayel, Y. W. Naguib, H. L. O'Mary, X. Li, M. Niu, T. B. Ruwona and Z. Cui, *Mol. Ther. - Nucleic Acids*, , DOI:10.1038/mtna.2016.39.
- 248 C. C. You, S. S. Agasti, M. De, M. J. Knapp and V. M. Rotello, *J. Am. Chem. Soc.*, 2006, **128**, 14612–14618.
- 249 R. Hong, T. Emrick and V. M. Rotello, *J. Am. Chem. Soc.*, 2004, **126**, 13572–13573.
- 250 M. Poreba and M. Drag, *Curr. Med. Chem.*, 2010, **17**, 3968–3995.
- 251 A. Kirchain, N. Poma, P. Salvo, L. Tedeschi, B. Melai, F. Vivaldi, A. Bonini, M. Franzini, L. Caponi, A. Tavanti and F. Di Francesco, *TrAC - Trends Anal. Chem.*, 2019, **110**, 35–50.
- 252 N. Gangloff, J. Ulbricht, T. Lorson, H. Schlaad and R. Luxenhofer, *Chem. Rev.*, 2016, **116**, 1753–1802.
- 253 Y. Luo, Y. Song, M. Wang, T. Jian, S. Ding, P. Mu, Z. Liao, Q. Shi, X. Cai, H. Jin, D. Du, W. Dong, C. Chen and Y. Lin, *Small*, 2019, **1902485**, 1902485.
- 254 A. S. Culf, *Biopolymers*, , DOI:10.1002/bip.23285.

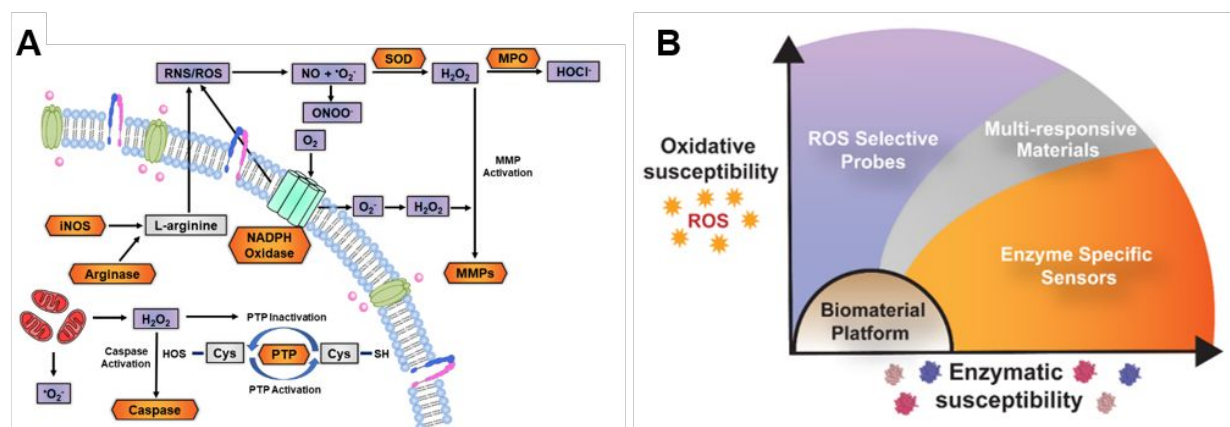


Figure 1. Landscape of cellular environment necessary for consideration in biosensor design. **(A)** Schematic representation of oxidative (purple) and enzymatic (orange) activity and their interplay within inflammatory microenvironments (Key: SOD = superoxide dismutase, MPO = myeloperoxidase, iNOS = nitric oxide synthase, PTP = protein tyrosine phosphatase). **(B)** Brainstorm of biomaterial design space for inspiration of biosensor engineering to address the entire spectra of inflammatory biomarkers encountered *in vivo*.

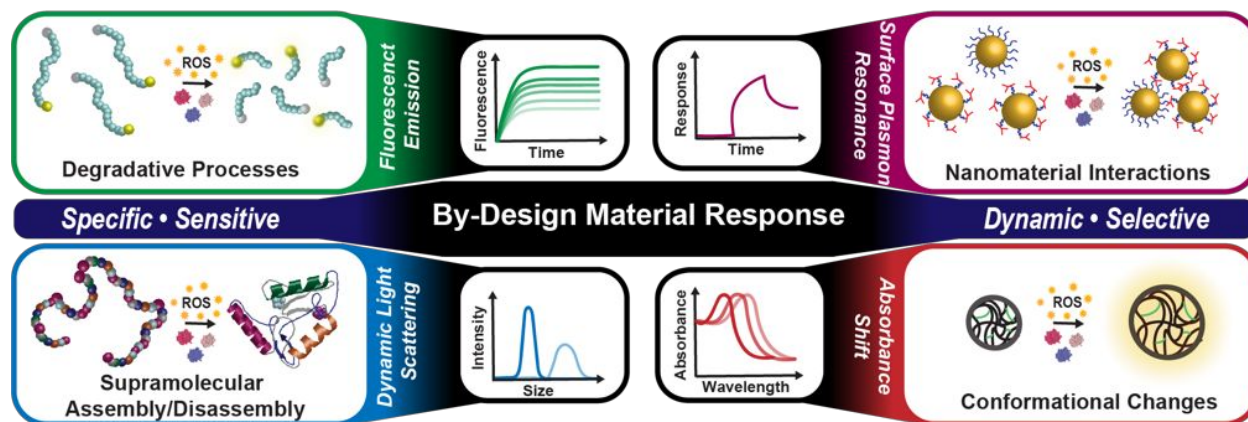


Figure 2. Material response classes and examples of corresponding sensing outputs amenable to *in vivo* application. An “ideal” biosensor is specific, sensitive, dynamic, and selective. Trade-offs in these criteria are often encountered, inviting consideration of novel materials chemistry approaches and design strategies to generate next generation biosensors.

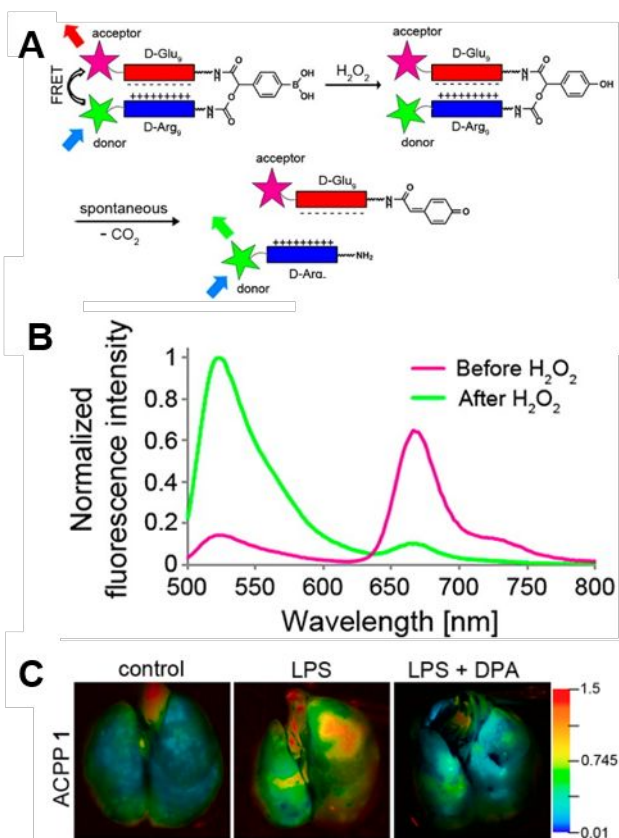


Figure 3. Oxidatively activated FRET degradation probe. **(A)** Reaction schematic of H₂O₂-reactive CPP. FRET quenching occurs when fluorophore moieties are in proximity then ceases upon H₂O₂-induced cleavage of the boronic acid linker, liberating the inhibitory polyanion (D-Glu₉) from the CPP (D-Arg₉). **(B)** FRET disruption visualized as the fluorescence shift from high wavelength (Cy5 acceptor, pink) to lower wavelength emission (fluorescein donor, green) upon cleavage. **(C)** Detection of endogenous H₂O₂ levels in lipopolysaccharide (LPS) model of mouse lungs scaled by emission ratio. Lungs of LPS-treated mice demonstrated a ~2-fold increase in fluorescein/Cy5 emission ratio compared to a control with no ACPP, as well as a control with D-penicillamine (LPS + DPA) added to scavenge H₂O₂. Adapted with permission from ref. 55. Copyright 2013 American Chemical Society.

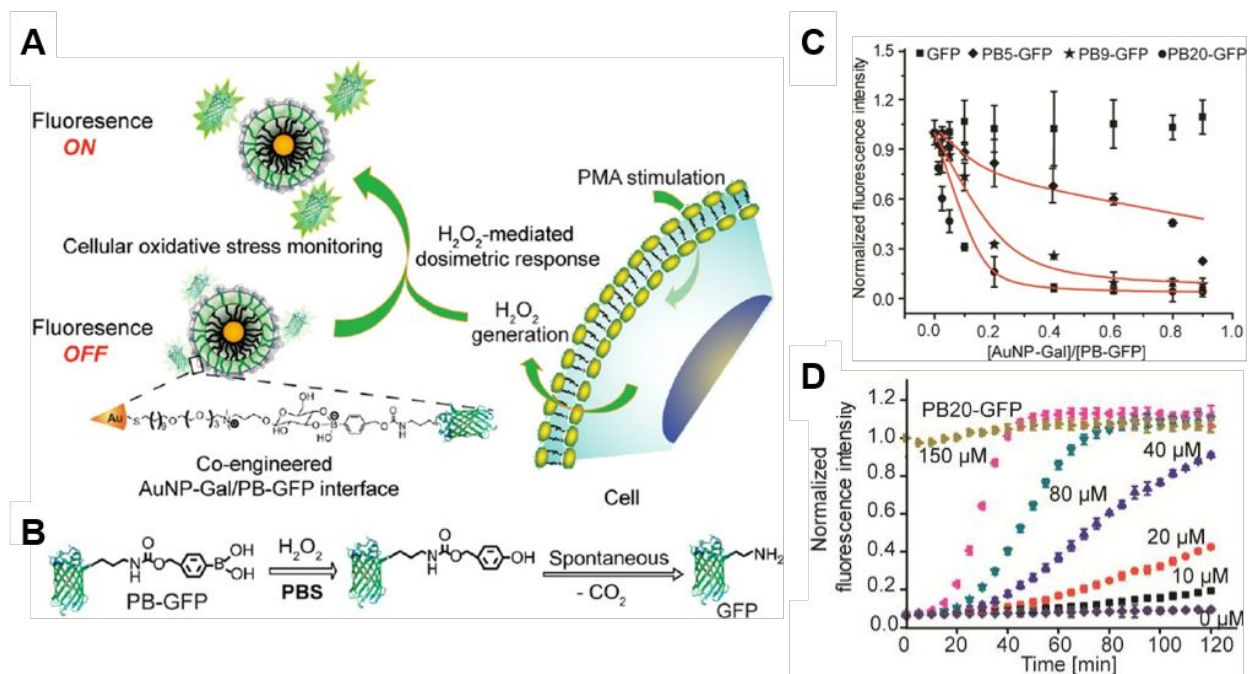


Figure 4. Hybrid nanomaterial degradation approach to sensing hydrogen peroxide. **(A)** Schematic representation of fluorescently engineered nanomaterial platform with PB-GFP affixed to AuNP-Gal for H_2O_2 detection *in situ*, stimulated by phorbol 12-myristate-13-acetate (PMA). **(B)** ROS-responsive reaction mechanism using bio-orthogonal boronate functionality to trigger molecular disassembly and release of GFP for fluorescence monitoring. **(C)** Chemical modulation of normalized fluorescent quenching using ratio of boronate moieties conjugated to GFP (represented as PB#-GFP to indicate # of PB per protein molecule). Fluorescence of the control GFP in solution is independent of AuNP-Gal concentration added, whereas PB-GFP fluorescence is quenched as a function of AuNP-Gal concentration and boronate functionalization. **(D)** Tunable, sensitive fluorescence response of PB20-GFP as a function of H_2O_2 concentration. Reprinted from ref. 52 with permission from John Wiley and Sons.

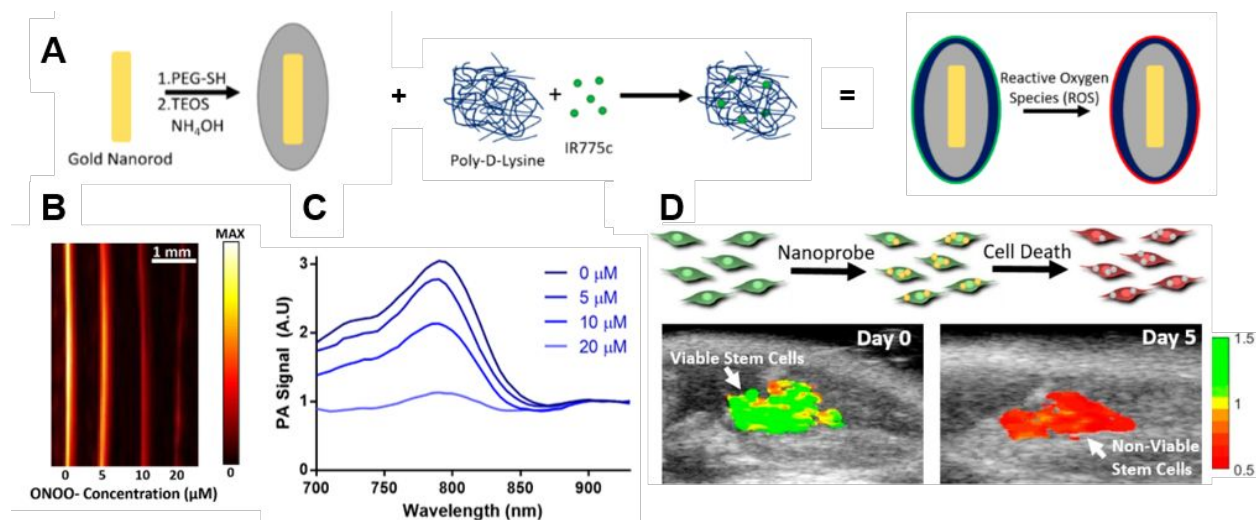


Figure 5. ROS detection utilizing ratiometric signal amplification. **(A)** Schematic representation of PA nanoprobe synthesis. PEGylated AuNRs are silica coated and bound to PDL and IR775c via electrostatic interactions. Following probe interaction with ROS, the dye degrades while the stable AuNR does not change, thereby providing different PA signals (green to red). **(B)** Upon exposure to ONOO⁻, the PA signal at 790 nm is reduced. **(C)** Upon exposure to ONOO⁻, the PA spectra shows differing responses for the dye peak (790 nm) and the AuNR peak (910 nm), enabling ratiometric detection. **(D)** Visualization of successful stem cell viability tracking *in vivo* using ratiometric imaging. Higher values on the ratiometric heat map (green, day 0) indicate living stem cell populations, while lower values indicate dying or dead populations (red, day 7). Adapted with permission from ref. 68. Copyright 2019 American Chemical Society.

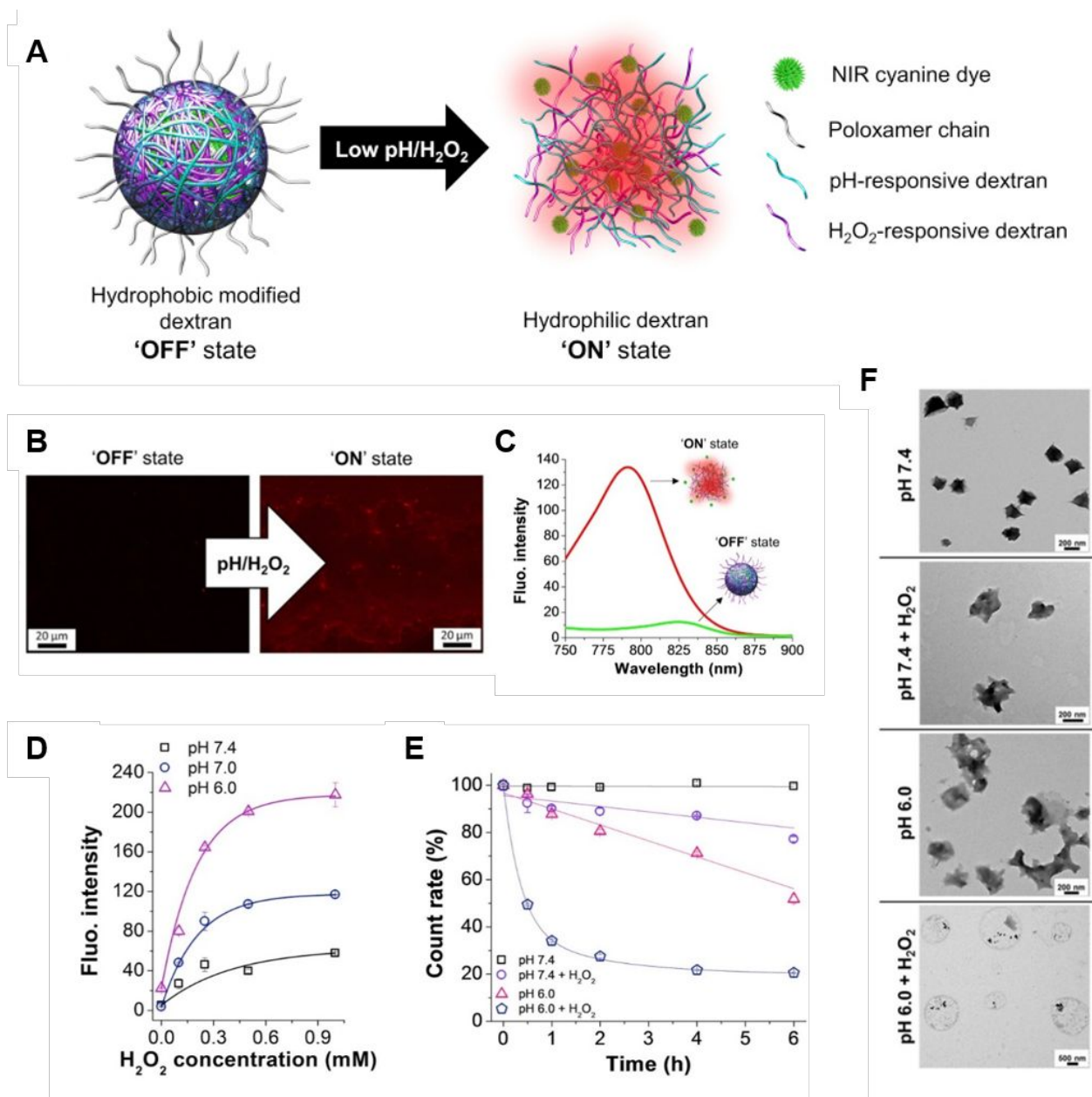


Figure 6. Dual-responsive H₂O₂/low pH nanoparticle system. **(A)** Illustration of pH/ROS-sensitive nanoprobe components for NIR imaging in inflammatory environments. **(B,C)** Detectible switching between the 'ON' and 'OFF' state as a function of low pH and H₂O₂ exposure is depicted in fluorescence microscopy images and emission spectra of the nanoprobe, respectively. **(D)** Sensitivity of the nanoprobe quantified by fluorescence intensity as a function of pH and H₂O₂ concentration. **(E,F)** Combined triggers showing synergistic degradation contributions of inflammatory environments by the percentage of nanoprobe in tact as function of time (quantified by DLS) and corresponding transmission electron micrograph (TEM) representations of the nanoprobe after two hours at 37°C in each condition, respectively. Reprinted from ref. 56 with permission from Elsevier.

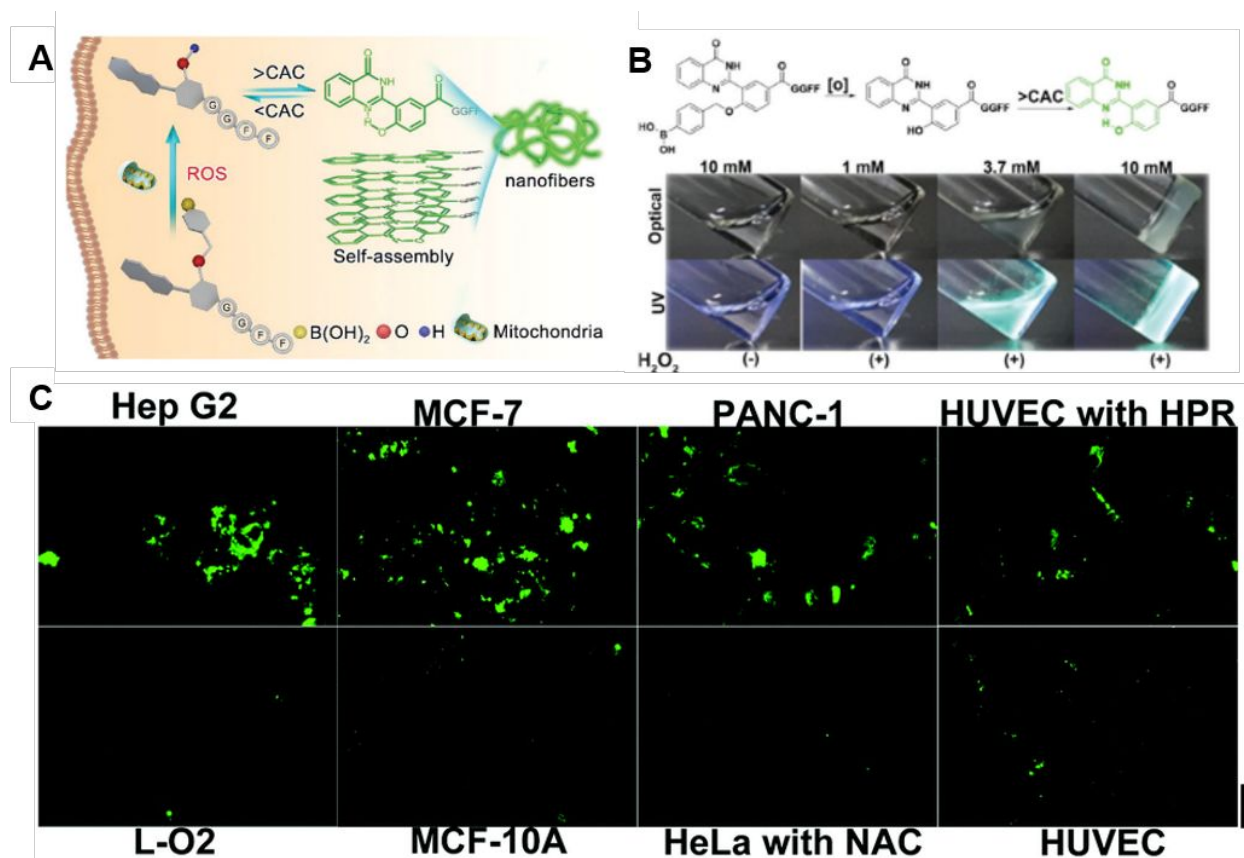


Figure 7. Dynamic fluorescence output enabled by supramolecular assembly system. **(A)** Schematic representation of oxidation-induced supramolecular self assembly of BQA connected to a tetra peptide chain (GGFF). Upon reaction with intracellular H_2O_2 , π - π stacking leads to nanofiber formation. **(B)** Fluorescence depends on CAC and hydrogelation concentration of BQA-GGFF in water at pH 7.4. As demonstrated, concentration of BQA-GGFF as high as 10 mM remained non-fluorescent without the addition of H_2O_2 . Upon addition of 3 equivalents of H_2O_2 (as indicated by +) the fluorescence significantly increases. **(C,D)** Fluorescence images of various cells incubated with 500 μM of BQA-GGFF. BQA-GGFF successfully distinguishes cancer cells (Top Panels: Hep G2, MCF-7, PANC-1,) from normal cells (Bottom Panels: L-O2, MCF-10A and HUVEC). This is confirmed by decreased fluorescence in the presence of normal HeLa + ROS inhibitor (*N*-acetyl-cysteine, NAC) and increased fluorescence in HUVEC cells in the presence of ROS inducer (4-hydroxyphenylretinamide, HPR). Scale bar: 20 μM . Reproduced from Ref. 85 with permission from The Royal Society of Chemistry.

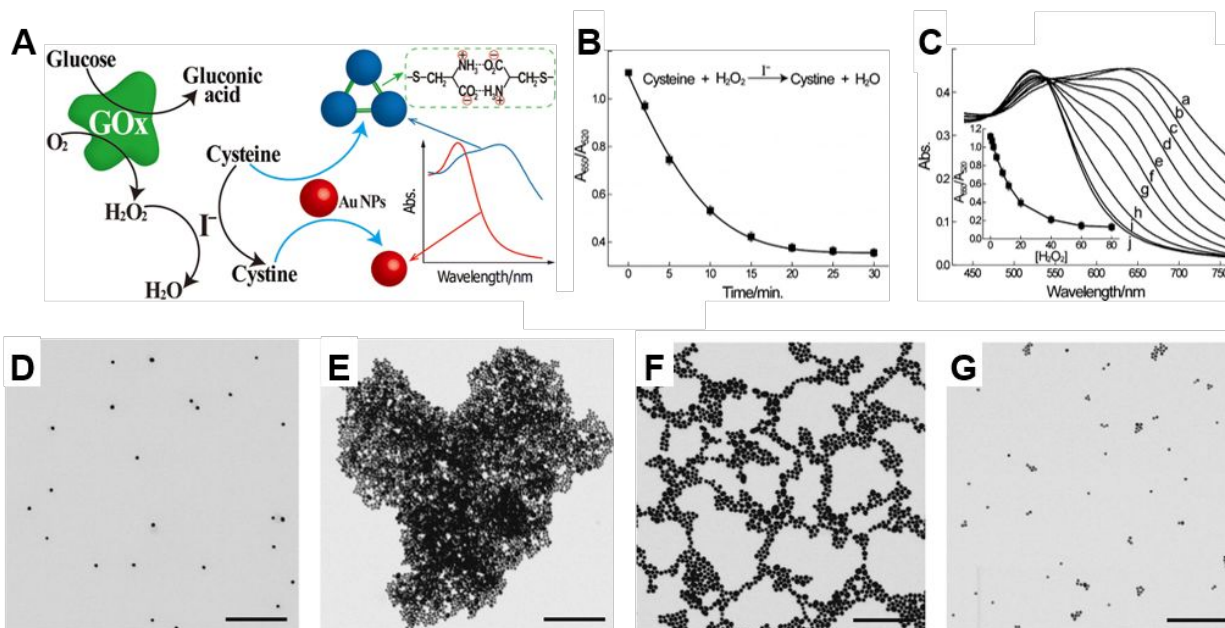


Figure 8. Reversible colorimetric sensor based on nanoparticle aggregation. **(A)** Schematic representation of oxidation-induced nanoparticle interactions and resulting absorbance shifts mediated through cysteine/cystine transformations **(B)** Characteristic time-dependent change in absorbance ratio of un-aggregated AuNPs (520 nm) to aggregated AuNPs (650nm) as a result of the iodide (I⁻) catalyzed oxidation of cysteine by H₂O₂ (20 μM) over 30 minutes **(C)** Absorbance shifts as a result of cysteine capped AuNPs treated with differing concentrations of H₂O₂ (a-j) corresponding to a range of 0-80 μM). I⁻ concentration was fixed at 2 μM. Inset is a calibration curve derived from the absorbance of the aggregated AuNPs and H₂O₂ concentration, demonstrating aggregation inhibition as H₂O₂ concentration increases. Analysis indicated a detection limit of 2 μM H₂O₂ **(D-G)** TEM images of AuNP aggregates resulting from treatment with H₂O₂. (D = bare AuNPs; E = no H₂O₂; F = 16 μM of H₂O₂ + 0.2 μM I⁻; G = 40 μM H₂O₂ + 0.2 μM I⁻). Reprinted with permission from ref. 86. Copyright 2013 American Chemical Society.

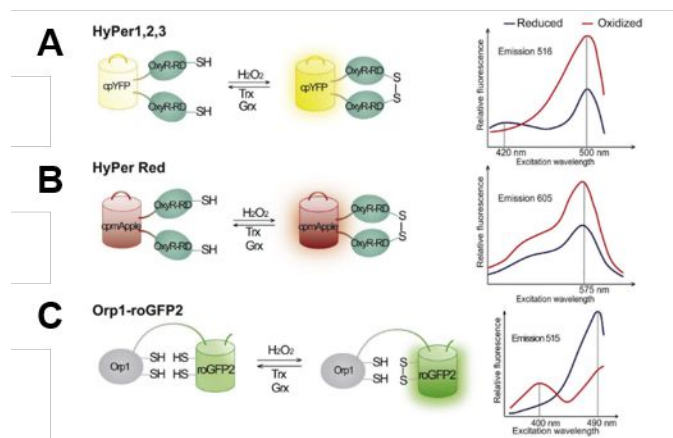


Figure 9. Genetically encoded fluorescent proteins as redox probes. *Left:* Schematic of the three most commonly used families of HyPer probes. *Right:* As illustrated, detection is achieved through ratiometric changes of emission and excitation peaks, dependent on oxidized and reduced forms of the HyPer constructs. **(A)** HyPer 1,2, and 3 probes based on circularly permuted yellow fluorescent proteins, cpYFP. **(B)** HyPer Red probes based on red fluorescent protein, cpmApple. **(C)** Orp1-roGFP2 based on redox sensitive green fluorescent proteins and yeast thiol peroxidase. Reprinted from ref. 91 with permission from Elsevier.

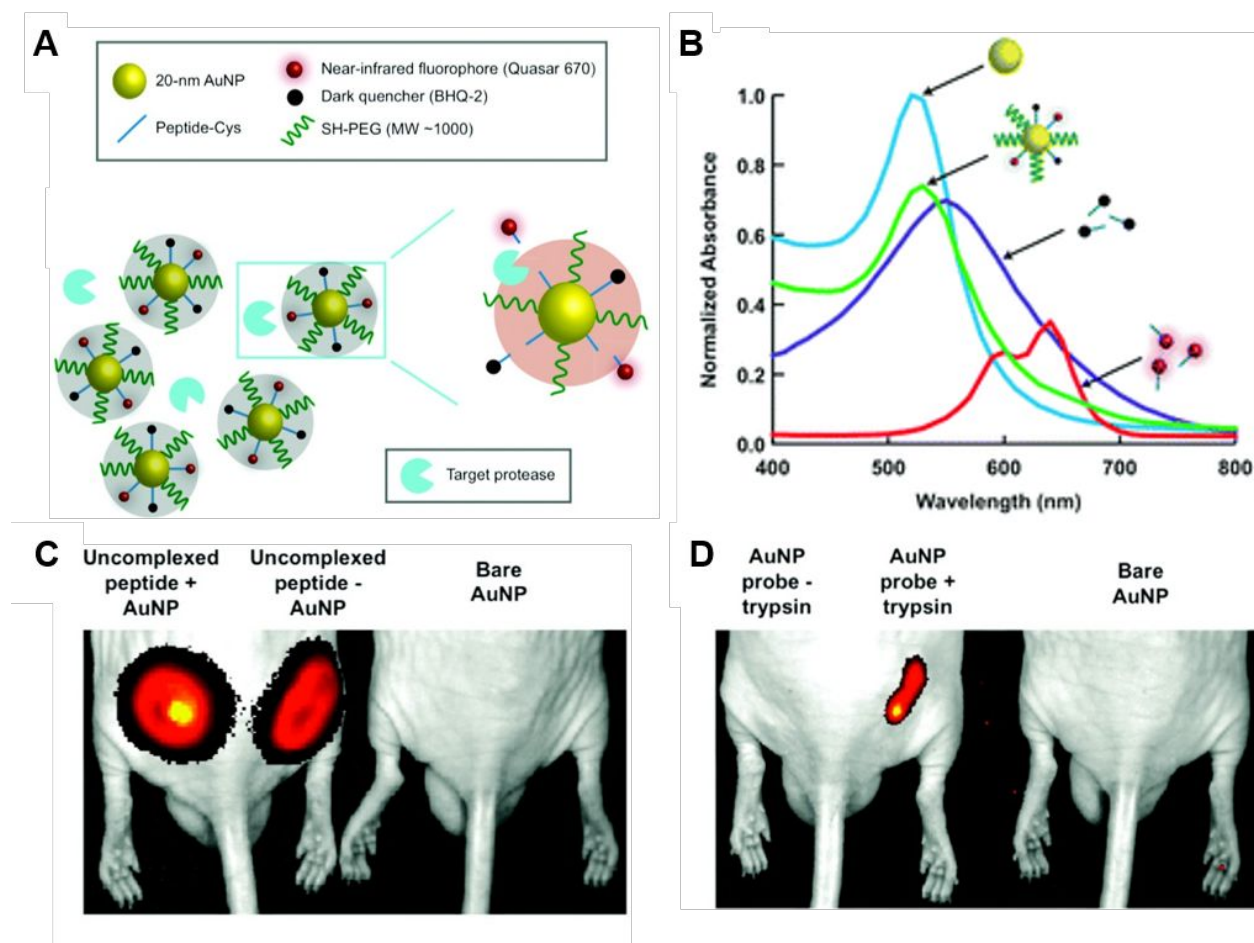


Figure 10. NIRF AuNP probe utilizing functional screens of trypsin and uPA-targeted libraries and validated *in vivo*. **(A)** Diagram of AuNP probes with unique peptide surface composition, selectively activated by the target protease. **(B)** Schematic illustration demonstrating method for signal detection based on differing absorbance spectra of AuNP probe components (top to bottom): bare AuNP (cyan curve), fully intact probe consisting of PEG and peptide labeled substrates (green curve), and liberated peptide substrates post enzymatic engagement (purple and red curves). As indicated by the differing purple and red signals, multiplexing is achieved through design of peptide linkers. **(C-D)** *In vivo* NIR imaging of tumor model. **(C)** Confirmation that presence of AuNPs in fully intact probe does not decrease fluorogenic peptide signal. **(D)** Activation of probes shown by a strong fluorescent signal in the presence of the target protease (250 U Trypsin), with no nonspecific activation by other biological species, as demonstrated by lack of signal for both the bare AuNPs and probes in the absence of trypsin. Reprinted with permission from ref. 166. Copyright 2010 American Chemical Society.

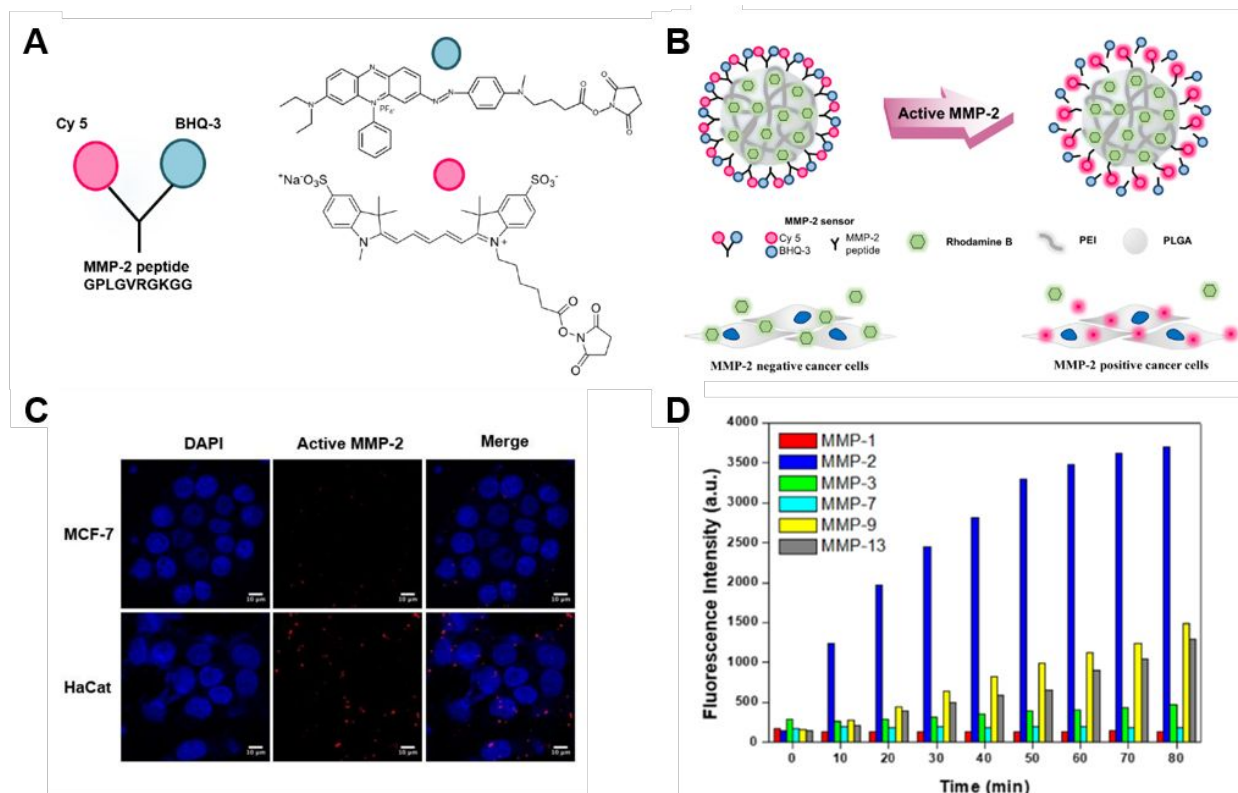


Figure 11. PLGA/PEI-based MMP-2 specific nanoparticle sensor with embedded rhodamine B for continuous monitoring of particle location. **(A)** Structure of MMP-2 sensitive peptide probe with Cy5 (NIR fluorophore, pink) and BHQ-3 (dark quencher, blue) installed as FRET moieties. **(B)** Graphic representation of MMP-2-PLGA-PEI nanoparticles reacting with activated MMP-2. In the absence of MMP-2 rhodamine B allows for particle tracking to localized environments. Cell excreting MMP-2 will cause the peptide linker to be cleaved and Cy5 to be released. **(C)** Confocal microscopy images of fluorescence signal recovery as a function of MMP-2 expression in MCF-7 (MMP-2 negative) and HaCat (MMP-2 positive) cell lines. After only 30 minutes of incubation, ~2-fold increase in Cy 5 fluorescence is observed and continues to increase with time. **(D)** Selectivity for MMP-2 is demonstrated by fluorescent response to peptide cleavage by various recombinant MMP types. Content reproduced from A. Lee *et al.*, distributed under the Creative Commons Attribution License, copyright 2018, accessible at <https://creativecommons.org/licenses/by/4.0/>.

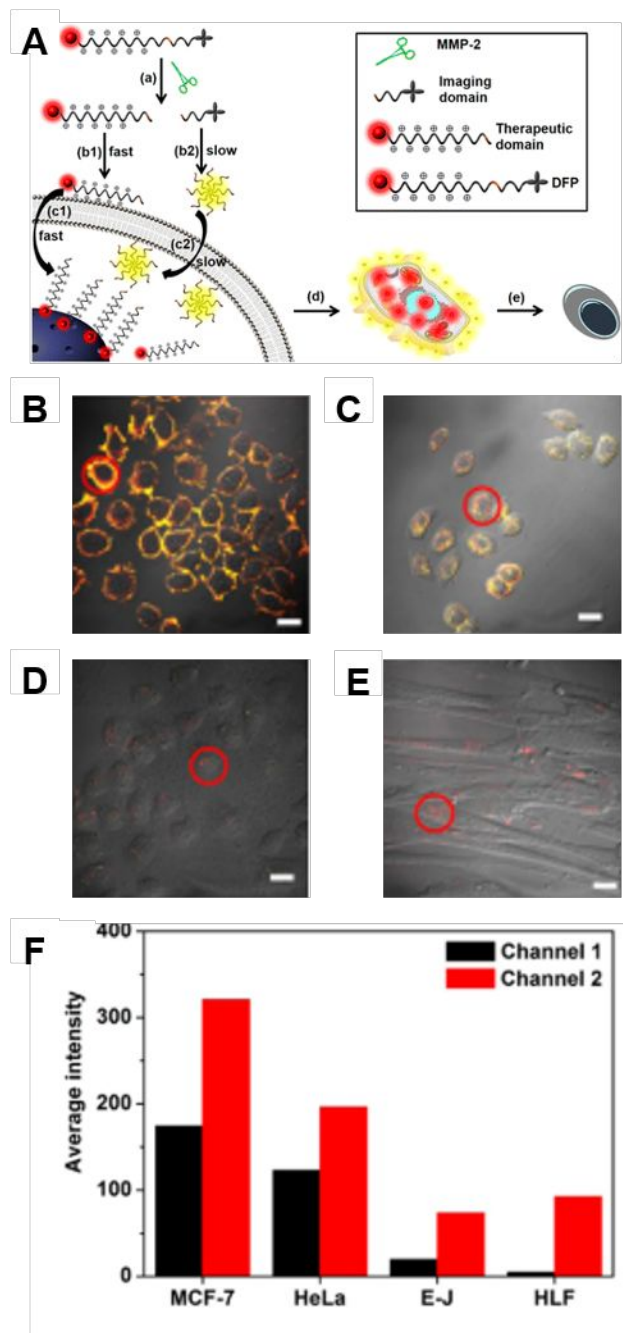


Figure 12. Protease-responsive cancer imaging probe and drug release platform. **(A)** Schematic representation of MMP-2 cleavable peptide sequence (LGLAG) with tethered DOX and PyTPE units. Cleavage of the peptide sequence (a) results in a DOX-linked CPP able to rapidly release DOX (b1) and diffuse into cells (c1), innately producing fluorescence signal (d) and killing the cells (e). On a slower timescale, the PyTPE-modified portion of the peptide linker self-aggregates and produces yellow fluorescence (b2, c2). **(B-E)** Cell lines with varying MMP-2 expression levels visually demonstrate the fluorescent response. (B = MCF-7 cells, high level MMP-2 expression; C = HeLa, high level MMP-2 expression; D = E-J cells, low level MMP-2 expression; E = HLF cells, low level MMP-2 expression). **(F)** Average fluorescence intensity in red circled region of interest for PyTPE fluorescence (495-575 nm, channel 1) and DOX (595-675 nm, channel 2). Adapted with permission from ref. 203. Copyright 2016 American Chemical Society. release DOX

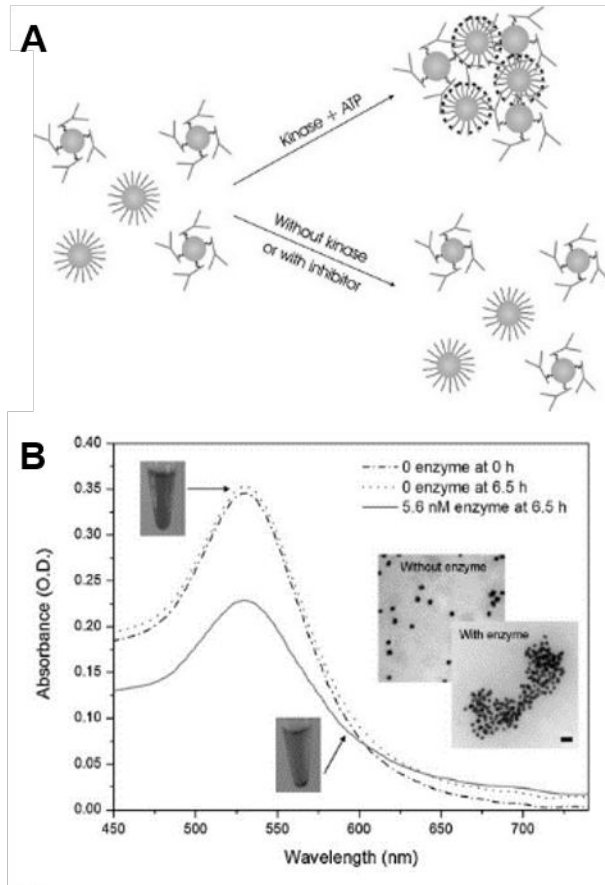


Figure 13. Single-step kinase sensing based on peptide-coated AuNP aggregation. **(A)** Graphic depiction of two particle populations, one coated in cysteine-bound Src-kinase peptide substrate (Ac-IYGEFKKKC) and the other with complementary antiphosphotyrosine antibodies. In the presence of kinase and ATP the peptide is phosphorylated, resulting in interparticle cross-linking. **(B)** UV-Vis spectra and TEM of NPs incubated with enzyme compared to controls. Particle aggregation causes a plasmon resonance red shift and ~30% decrease in absorbance intensity after 6.5 hours as a result of precipitated clusters. Reprinted from ref. 223 with permission from John Wiley and Sons.

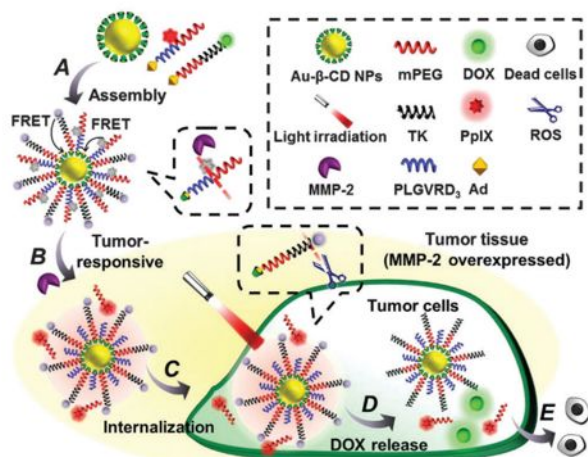


Figure 14. Dual-responsive AuNP theranostic platform targeting MMP-2 overexpression in tumor cells. β -cyclodextrin-coated AuNPs are conjugated to reactive probes with adamantane (Ad) linkers via host-guest interactions and quench fluorescence of bound fluorophores (A). PEG chains with an MMP-2 cleavable linker are used to release protoporphyrin IX (ppIX), a photosensitizer, for tumor tissue imaging in the inflammatory environment with upregulated MMP-2 (B). The NPs and freed ppIX are then internalized (C) and irradiated to degrade TK and release DOX on-demand (D), causing apoptosis of tumor cells (E). Reproduced from ref. 80 with permission from The Royal Society of Chemistry.

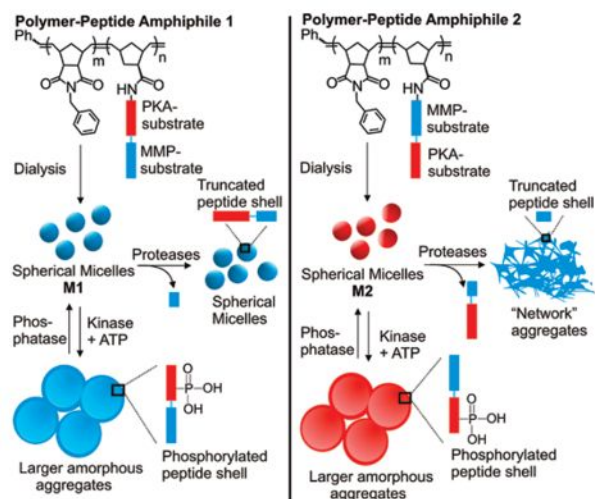


Figure 15. Polymer-peptide amphiphile nanoparticles with enzyme-directed morphological switches. Spherical micelles were formed using block copolymers with peptide brushes responsive to kinase degradation (PKA-substrate, red) and proteolysis (MMP-substrate, blue) incorporated onto the hydrophilic head. By changing the relative ordering of substrates bound to the polymer backbone, the corona and shell of the micelle are able to be effectively functionalized by design. In both cases, micelles treated with kinase and ATP are phosphorylated, leading to large amorphous aggregates, which can then be reverted back to defined micelles when dephosphorylated by protein phosphatase 1. When the MMP-substrate is added second the micelles remain intact upon exposure to MMP-2 and MMP-9. When the micelle corona is made up of MMP-substrate, however, proteolysis disrupts the micellar structure and leads to an amorphous network of aggregates. Reprinted with permission from ref. 204. Copyright 2011 American Chemical Society.

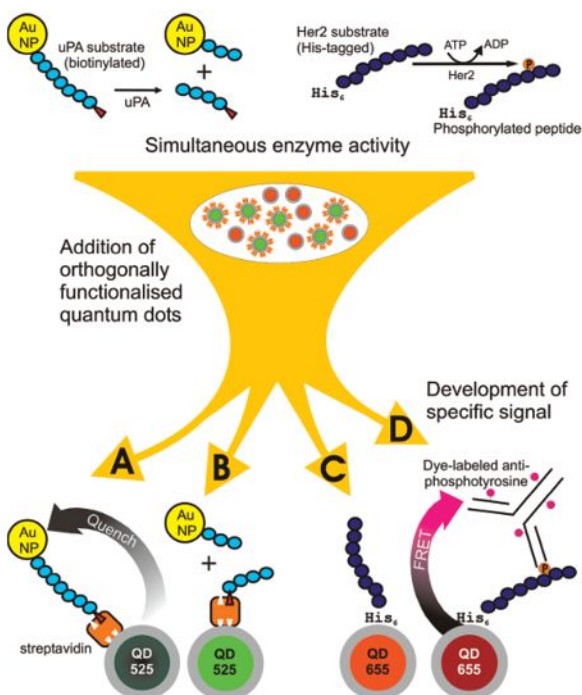


Figure 16. Specific enzyme detection via orthogonal functionalization to photoluminescent QDs. This multicomponent solution-based assay is able to detect uPA and Her2. Enzyme-specific detection was enabled using amino acid recognition sequences selective to each enzyme, orthogonal conjugation chemistry, QDs with distinct emission spectra and inverse FRET behavior. The uPA probe (blue, sequence SGRSAN) was biotinylated on the N-terminus for coupling to streptavidin-labeled QD525 and C-terminally covalently attached to an AuNP using a cysteine residue. When conjugated, the AuNP quenches luminescence (A) allowing for disruption of FRET upon hydrolytic cleavage with uPA and detectible photoluminescence (B). The Her2 responsive component (purple, sequence DNEY*FYV, star indicates phosphorylated residue) includes an N-terminal His tag with affinity for ZnS shell of QD655 and spacer glycine residues to enable antibody accessibility. The QD is initially luminescent (C), but is quenched when a dye-labeled antibody is bound as an acceptor moiety (D). Reprinted with permission from ref. 173. Copyright 2012 American Chemical Society.